Articles

Dissociative CO Photosubstitution in $M(CO)_4$(1,4-diazabutadiene) Complexes (M = W, Mo) by an Olefin Affording Novel *fac*-$M(CO)_3$(1,4-diazabutadiene)(η^2-olefin) Derivatives

Friedrich-Wilhelm Grevels,* Klaus Kerpen, Werner E. Klotzbücher, and Kurt Schaffner

Max-Planck-Institut für Strahlenchemie, Postfach 10 13 65, D-45413 Mülheim an der Ruhr, Germany

Richard Goddard and Bruno Weimann

Max-Planck-Institut für Kohlenforschung, Kaiser-Wilhelm-Platz 1, D-45470 Mülheim an der Ruhr, Germany

Ceyhan Kayran and Saim Özkar*

Department of Chemistry, Middle East Technical University, 06531 Ankara, Turkey

Received May 17, 2001

Photolysis of $M(CO)_4$(iprop-dab) (**1**, M = W; **2**, M = Mo; iprop-dab = 1,4-diisopropyl-1,4-diazabuta-1,3-diene) in the presence of (*E*)-cyclooctene (eco) afforded high yields of the unprecedented olefin-substituted derivatives *fac*-$M(CO)_3$(iprop-dab)(η^2-eco) (**3**, M = W, 93%; **4**, M = Mo, 84%), which were comprehensively characterized by IR, UV−vis, and NMR spectroscopy and by an X-ray diffraction structure analysis of **3**. Quantum yield measurements at 254, 302, 365, and 405 nm revealed a gradual decrease from $\Phi \approx 0.1$ to 0.02 and then a sharp drop to 0.001 at 548 nm (CTML excitation). Irradiation of **2** in low-temperature matrices, as monitored by means of IR spectroscopy in the ν(CO) region, was shown to yield *fac*-$Mo(CO)_3$(iprop-dab) (**5**, in Ar or CO-doped Ar), *fac*-$Mo(CO)_3(^{13}CO)$(iprop-dab) (in ^{13}CO-doped Ar), and *fac*-$Mo(CO)_3(N_2)$(iprop-dab) (**6**, in N_2), thereby establishing that a vacant axial coordination site is created by photolytic CO dissociation, with wavelength-dependent efficiency. The involvement of the (solvated) fragment *fac*-$M(CO)_3$(iprop-dab) as a key intermediate in the solution photochemistry of $M(CO)_4$(iprop-dab) was substantiated by laser flash photolysis of **2** in combination with time-resolved IR and UV−vis spectroscopy. ^{13}CO-enriched samples of **1** and **2** (specifically monolabeled) as well as **3**, **5**, and **6** (partially labeled) were used for gathering complementary ν(CO) data as a basis for energy-factored CO force field analyses. The response of the low-energy CTML electronic transitions to the loss of CO and its replacement by the olefin or N_2 ligand is discussed in terms of ligand-dependent metal d(π) level stabilization.

Introduction

The photochemistry and photophysical properties of group 6 $M(CO)_4$(α-diimine) complexes (M = Cr, Mo, W) have been extensively investigated. As a common feature of this class of compounds, the electronic absorption spectra exhibit prominent bands in the visible region which are attributed to transitions thought to be mainly metal (d)→ligand (π*) charge-transfer (MLCT) in character, as concluded from solvatochromic effects, resonance Raman excitation profiles, and emission spectra.[1−24]

* To whom correspondence should be addressed. E-mail: F.-W.G., grevels@mpi-muelheim.mpg.de; S.Ö., sozkar@metu.edu.tr.

(1) Bock, H.; tom Dieck, H. *Chem. Ber.* **1967**, *100*, 228−246.
(2) tom Dieck, H.; Renk, I. W. *Angew. Chem.* **1970**, *82*, 805−807. *Angew. Chem., Int. Ed. Engl.* **1970**, *9*, 805−807.
(3) tom Dieck, H.; Renk, I. W. *Chem. Ber.* **1971**, *104*, 110−130.
(4) Brunner, H.; Herrmann, W. A. *Chem. Ber.* **1972**, *105*, 770−783.
(5) Renk, I. W.; tom Dieck, H. *Chem. Ber.* **1972**, *105*, 1403−1418.
(6) tom Dieck, H.; Franz, K.-D.; Hohmann, F. *Chem. Ber.* **1975**, *108*, 163−173.
(7) Wrighton, M. S.; Morse, D. L. *J. Organomet. Chem.* **1975**, *97*, 405−420.
(8) Balk, R. W.; Stufkens, D. J.; Oskam, A. *J. Chem. Soc., Chem. Commun.* **1978**, 1016−1017.
(9) Staal, L. H.; Stufkens, D. J.; Oskam, A. *Inorg. Chim. Acta* **1978**, *26*, 255−262.

10.1021/om010410b CCC: $20.00
Publication on Web 10/12/2001

Photosubstitution of CO with formation of *fac*-$M(CO)_3$(α-diimine)(L) products was studied with a variety of n-donor ligands L. It occurs with low to modest quantum yields,[7,13,18,23,25−33] depending on the wavelength of excitation, the metal, the type of α-diimine ligand, the properties of the entering ligand L, and other experimental conditions such as pressure, temperature, and concentration. Both dissociative and associative mechanisms were found to be operative. In general, the substitution leads to a significant bathochromic shift of the MLCT transitions,[5,6,10,13,25−27,30−32] consistent with the notion of a destabilization of metal (d) levels upon replacement of a strongly π-accepting ligand, CO, by an entering ligand L with little, if any, π-acceptor ability.

Olefin ligands have not yet been examined in this respect, although a few $M(CO)_3$(α-diimine)(η^2-olefin) and $M(CO)_2$(α-diimine)(η^2-olefin)$_2$ complexes are known.[34−39] However, these compounds were prepared via non-photochemical routes and no UV−vis spectral data were reported. This lack of information, along with our continued interest in the photochemical synthesis and structural aspects of olefin-substituted group 6 metal carbonyls,[40−48] led us to launch an exploratory investigation into the photolytic behavior of $M(CO)_4$(α-diimine) complexes in the presence of an olefin. In this paper we report on the photoinduced reaction of $M(CO)_4$(iprop-dab) (M = W, Mo; iprop-dab = 1,4-diisopropyl-1,4-diazabuta-1,3-diene) with (*E*)-cyclooctene (eco) and on the structure and properties of the resulting $M(CO)_3$(iprop-dab)(η^2-eco) products. (*E*)-Cyclooctene was chosen as the entering olefin ligand because of its superior coordination ability.[41,42,44,47−52] The chosen type of an aliphatic α-diimine ligand, instead of aromatic congeners such as 2,2′-bipyridine and 1,10-phenanthroline type α-diimines, provides for better solubility of the complexes in alkane solvents and thus facilitates the intended investigation of the photochemistry in solution.

Results

Photochemical Synthesis and Thermal Reactivity of *fac*-$M(CO)_3$(iprop-dab)(η^2-eco). Photolysis of $M(CO)_4$(iprop-dab) (**1**, M = W; **2**, M = Mo) in the presence of excess (*E*)-cyclooctene generates the corresponding olefin-substituted derivatives *fac*-$M(CO)_3$(iprop-dab)(η^2-eco) (**3**, M = W; **4**, M = Mo; eco = (*E*)-cyclooctene) (Scheme 1), which are identified on the basis of analytical and spectroscopic data (vide infra). The best yields are obtained in cyclohexane solution, which, compared with other alkane solvents, provides for higher solubility of both the starting materials and the products.

Scheme 1

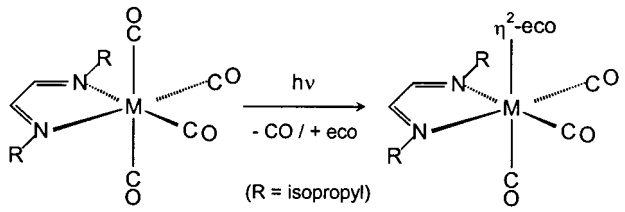

1 (M = W) **3** (M = W)
2 (M = Mo) **4** (M = Mo)

Monitoring the progress of these reactions by means of IR spectroscopy (vide infra) shows that, in either case, the *fac*-$M(CO)_3$(iprop-dab)(η^2-eco) complex remains the only detectable product until the starting material has completely vanished. Further irradiation beyond this point leads to gradual, albeit slow, photodecomposition

(10) Balk, R. W.; Stufkens, D. J.; Oskam, A. *Inorg. Chim. Acta* **1978**, *28*, 133−143.
(11) Balk, R. W.; Stufkens, D. J.; Oskam, A. *Inorg. Chim. Acta* **1979**, *34*, 267−274.
(12) Balk, R. W.; Stufkens, D. J.; Oskam, A. *J. Chem. Soc., Chem. Commun.* **1979**, 604−605.
(13) Balk, R. W.; Snoeck. T.; Stufkens, D. J.; Oskam, A. *Inorg. Chem.* **1980**, *19*, 3015−3021.
(14) Stufkens, D. J. *J. Mol. Struct.* **1982**, *79*, 67−82.
(15) Manuta, D. M.; Lees, A. J. *Inorg. Chem.* **1983**, *22*, 3825−3828.
(16) Servaas, P. C.; van Dijk, H. K.; Snoeck, T. L.; Stufkens, D. J.; Oskam, A. *Inorg. Chem.* **1985**, *24*, 4494−4498.
(17) Macholdt, H.-T.; van Eldik, R.; Kelm, H.; Elias, H. *Inorg. Chim. Acta* **1985**, *104*, 115−118.
(18) Manuta, D. M.; Lees, A. J. *Inorg. Chem.* **1986**, *25*, 1354−1359.
(19) Manuta, D. M.; Lees, A. J. *Inorg. Chem.* **1986**, *25*, 3212−3218.
(20) Ernst, S.; Kurth, Y.; Kaim, W. *J. Organomet. Chem.* **1986**, *302*, 211−215.
(21) Kaim, W.; Kohlmann, S. *Inorg. Chem.* **1986**, *25*, 3306−3310.
(22) Rawlins, K. A.; Lees, A. J. *Inorg. Chem.* **1989**, *28*, 2154−2160.
(23) Stufkens, D. J. *Coord. Chem. Rev.* **1990**, *104*, 39−112.
(24) Kaim, W.; Kohlmann, S.; Lees, A. J.; Snoeck, T. L.; Stufkens, D. J.; Zulu, M. M. *Inorg. Chim. Acta* **1993**, *210*, 159−165.
(25) van Dijk, H. K.; Servaas, P. C.; Stufkens, D. J.; Oskam, A. *Inorg. Chim. Acta* **1985**, *104*, 179−183.
(26) Wieland, S.; van Eldik, R. *J. Chem. Soc., Chem. Commun.* **1989**, 367−369.
(27) Wieland, K.; Reddy, K. B.; van Eldik, R. *Organometallics* **1990**, *9*, 1802−1806.
(28) Víchová, J.; Hartl, F.; Vlček, A., Jr. *J. Am. Chem. Soc.* **1992**, *114*, 10903−10910.
(29) Lindsay, E.; Vlček, A., Jr.; Langford, C. H. *Inorg. Chem.* **1993**, *32*, 2269−2275.
(30) Fu, W.-F.; van Eldik, R. *Inorg. Chim. Acta* **1996**, *251*, 341−346.
(31) Fu, W.-F.; van Eldik, R. *Organometallics* **1997**, *16*, 572−578.
(32) Fu, W.-F.; van Eldik, R. *Inorg. Chem.* **1998**, *37*, 1044−1050.
(33) Vlček, A., Jr. *Coord. Chem. Rev.* **1998**, *177*, 219−256.
(34) Schaper, H.; Behrens, H. *J. Organomet. Chem.* **1976**, *113*, 377−386.
(35) Lai, C.-H.; Cheng, C.-H.; Chou, W.-C.; Wang, S.-L. *Organometallics* **1993**, *12*, 1105−1112.
(36) Lai, C.-H.; Cheng, C.-H.; Chou, W.-C.; Wang, S.-L. *Organometallics* **1993**, *12*, 3418−3425.
(37) Lai, C.-H.; Cheng, C.-H. *Organometallics* **1993**, *12*, 3561−3564.
(38) Lai, C.-H.; Cheng, C.-H.; Liao, F.-L.; Wang, S.-L. *Inorg. Chem.* **1993**, *32*, 5658−5664.
(39) Zanello, P.; Laschi, F.; Fontani, M.; Mealli, C.; Ienco, A.; Tang, K.; Jin, X.; Li, L. *J. Chem. Soc., Dalton Trans.* **1999**, 965−970.
(40) Grevels, F.-W.; Lindemann, M.; Benn, R.; Goddard, R.; Krüger, C. *Z. Naturforsch., B* **1980**, *35*, 1298−1303.
(41) Grevels, F.-W.; Skibbe, V. *J. Chem. Soc., Chem. Commun.* **1984**, 681−683.
(42) Angermund, K.; Grevels, F.-W.; Krüger, C.; Skibbe, V. *Angew. Chem.* **1984**, *96*, 911−913; *Angew. Chem., Int. Ed. Engl.* **1984**, *23*, 904−905.
(43) Grevels, F.-W.; Jacke, J.; Özkar, S. *J. Am. Chem. Soc.* **1987**, *109*, 7536−7537.
(44) Grevels, F.-W.; Jacke, J.; Klotzbücher, W. E.; Özkar, S.; Skibbe, V. *Pure Appl. Chem.* **1988**, *60*, 1017−1024.
(45) Grevels, F.-W.; Jacke, J.; Betz, P.; Krüger, C.; Tsay, Y.-H. *Organometallics* **1989**, *8*, 293−298.
(46) Chmielewski, D.; Grevels, F.-W.; Jacke, J.; Schaffner, K. *Angew. Chem.* **1991**, *103*, 1361−1363; *Angew. Chem., Int. Ed. Engl.* **1991**, *30*, 1343−1345.
(47) Grevels, F.-W. In *Photoprocesses in Transition Metal Complexes, Biosystems and other Molecules: Experiments and Theory*; Kochanski, E., Ed.; Kluwer: Dordrecht, The Netherlands, 1992; pp 141−171.
(48) Grevels, F.-W.; Jacke, J.; Klotzbücher, W. E.; Mark, F.; Skibbe, V.; Schaffner, K.; Angermund, K.; Krüger, C.; Lehmann, C. W.; Özkar, S. *Organometallics* **1999**, *18*, 3278−3293.
(49) Ball, R. G.; Kiel, G.-Y.; Takats, J.; Krüger, C.; Raabe, E.; Grevels, F.-W.; Moser, R. *Organometallics* **1987**, *6*, 2260−2261.
(50) Angermund, H.; Grevels, F.-W.; Moser, R.; Benn, R.; Krüger, C.; Romão, M. J. *Organometallics* **1988**, *7*, 1994−2004.
(51) Angermund, H.; Bandyopadhyay, A. K.; Grevels, F.-W.; Mark, F. *J. Am. Chem. Soc.* **1989**, *111*, 4656−4661.
(52) Klassen, J. K.; Yang, G. K. *Organometallics* **1990**, *9*, 874−876.

of *fac*-M(CO)$_3$(iprop-dab)(η^2-eco) but does not cause secondary photosubstitution with formation of disubstituted products, in contrast to recent observations made upon extended photolysis of M(CO)$_4$(phen) complexes in the presence of PR$_3$ ligands.[30−32]

Once isolated as solid materials, both **3** and **4** are sufficiently stable for handling at ambient temperature, although cooling is recommended for long-term storage. In solution, however, this is only true for the tungsten complex **3**, while solutions of the molybdenum compound **4** have to be kept well below 0 °C in order to prevent it from thermal decomposition with loss of the olefin ligand. Spectroscopic measurements can nevertheless be performed at ambient temperature, provided that an excess of free (*E*)-cyclooctene is present.

Deliberate replacement of η^2-eco by CO or other ligands occurs thermally under mild conditions and can be exploited for synthetic purposes. Thus, treatment of **3** (at 40 °C) and **4** (at ambient temperature) with ^{13}CO in cyclohexane containing no added (*E*)-cyclooctene yields the specifically monolabeled (≥90% isotopic purity, by MS) M(CO)$_3$(^{13}CO)(iprop-dab) complexes **1-*1*** and **2-*1***,[53] respectively, which are formed as equimolar mixtures of the positional isotopomers carrying the single ^{13}CO group in either an axial (**1-*1a*, 2-*1a***) or an equatorial position (**1-*1e***, **2-*1e***) (Scheme 2). The ν(CO) data of these species,[54] along with those of the unlabeled compounds and the CO force and interaction constants evaluated therefrom at the level of the energy-factored CO force field approximation,[55−60] are listed in Table 1. The results compare very well with those of a previous study[61] in which ca. 1:1 mixtures of the unlabeled and monolabeled complexes were investigated.

Scheme 2

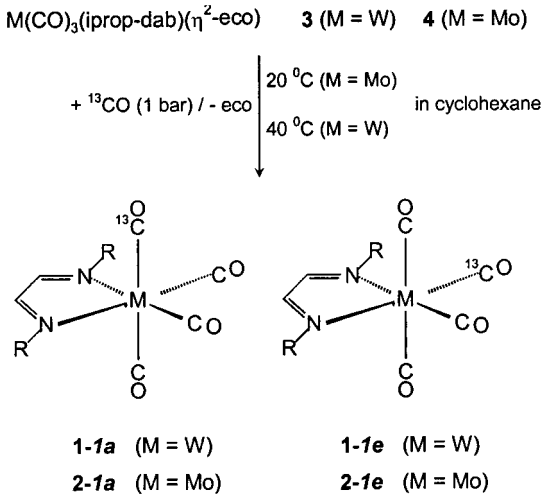

Characterization by IR and NMR Spectroscopy. The shape of the CO stretching vibrational spectra of **3** and **4** (Figure 1) is more compatible with a *fac*-M(CO)$_3$(L−L)(L′) type of complex than with a structure containing a *mer*-M(CO)$_3$ unit. The former commonly exhibits three ν(CO) bands with comparable intensities,[34,62−65] while the latter gives rise to a distinctly different intensity pattern, viz., a weak high-frequency band followed by two absorptions of medium and high intensity, respectively, at lower frequencies.[45,55,62,66,67] This leads us to propose the *fac*-M(CO)$_3$(iprop-dab)(η^2-olefin) structure shown in Scheme 1, where the olefin occupies an axial coordination site in a position cis to the chelate α-diimine ligand.

The molybdenum complex **4** apparently exists as a nearly equimolar mixture of two closely related isomers, since close inspection of its ν(CO) spectrum (Figure 1, bottom) reveals that two three-band patterns are present with separations ranging from 2 to 7 cm^{-1}. A second species may also be present as a component, albeit minor, in solutions of the tungsten complex **3**, because the three dominant ν(CO) bands (Figure 1, top) each show a barely discernible shoulder at the low-frequency side.

These isomers presumably differ in the orientation of the η^2-eco ligand with respect to the M(CO)$_2$(iprop-dab) plane. In two of the geometries sketched out in Scheme 3, **A** and **C**, the C═C bond of the olefin is eclipsed by one of the N−W−CO axes. This structural

(53) Italic numbers attached to a compound number indicate how many carbonyl positions are isotopically labeled by ^{13}CO. Lowercase letters indicate the position of ^{13}CO in the various stereoisotopomers (***a*** = axial, ***e*** = equatorial position). The symbol **#** denotes mixtures of isotopomers.

(54) For the sake of accuracy, the positions of closely spaced bands have been assessed by means of computer-assisted curve fitting using the appropriate options of the GRAMS/32 (V4.0) software package; Galactic Industries Corp., 395 Main Street, Salem, NH 03079.

(55) Braterman, P. S. *Metal Carbonyl Spectra*; Academic Press: London, 1975.
(56) Cotton, F. A.; Kraihanzel, C. S. *J. Am. Chem. Soc.* **1962**, *84*, 4432−4438.
(57) Haas, H.; Sheline, R. K. *J. Phys. Chem.* **1967**, *47*, 2996−3021.
(58) Bor, G. *Inorg. Chim. Acta* **1967**, *1*, 81−92.
(59) Bor, G. *J. Organomet. Chem.* **1967**, *10*, 343−359.

(60) A computer program written in Fortran 77 has been used to calculate the energy-factored CO force field parameters k_{CO} and $k_{CO,CO}$ from the experimentally available frequency data. Adapting Bor's notation,[58,59] the secular equation $|\mathbf{F} - \lambda\mathbf{G}^{-1}| = 0$ is written as $|\mathbf{F}_{CO} - y\mathbf{E}| = 0$ with $y = [4\cdot\pi^2 c_o^2 \mu_{CO}(\tilde{\nu}_{CO})^2]/N_A = (4.0396 \times 10^{-4})(\tilde{\nu}_{CO})^2$, where the units are cm^{-1} for $\tilde{\nu}_{CO}$ and N m^{-1} for *y* (calculated with $m(^{12}C) = 12.000\ 0$ g mol^{-1}, $m(^{13}C) = 13.003\ 355$ g mol^{-1}, $m(^{16}O) = 15.994\ 915$ g mol^{-1}, $c_o = 2.997\ 924\ 58 \times 10^8$ m s^{-1}, $N_A = 6.022\ 045 \times 10^{23}$ mol^{-1}. Data were taken from: Weast, R. C.; Astle, M. J.; Beyer, W. H. *CRC Handbook of Chemistry and Physics*; CRC Press: Boca Raton, FL, 1985. For the case of a $^{13}C^{16}O$-substituted isotopomer these equations are formulated as $|\mathbf{A}^{1/2}\mathbf{F}_{CO}\mathbf{A}^{1/2} - {}^*y\mathbf{E}| = 0$ or $|{}^*\mathbf{F}_{CO} - {}^*y\mathbf{E}| = 0$ where **A** is a diagonal matrix containing $a = \mu_{CO}/{}^*\mu_{CO} = 0.955\ 91$ in the $^{13}C^{16}O$-substituted positions and $a = 1$ in the others. The program considers preset upper and lower limits for both the diagonal and off-diagonal elements of $\mathbf{F}_{CO}$. For each element a finite number of equidistant values are taken, and all combinations of these values are forming a grid. For each node of this grid the eigenvalues of $\mathbf{F}_{CO}$ and ${}^*\mathbf{F}_{CO}$ are calculated. When these calculated eigenvalues are compared with the experimental *y* and ***y*** values, the variance is determined, and the node with the lowest variance is the center of a new, smaller grid until a given lower limit for the size of the grid is reached. Starting with the center of this grid, the method of steepest descent is used to find the minimum of variance: i.e., to find those values of the $\mathbf{F}_{CO}$ matrix elements which give the best fit to the experimental $\tilde{\nu}_{CO}$ and ${}^*\tilde{\nu}_{CO}$ data. Information on the symmetry of the carbonylmetal unit is introduced, if applicable, in the form of the indices of those $\mathbf{F}_{CO}$ matrix elements which have to be taken as identical, such that only a subset of them has to be determined. In addition to the final $\mathbf{F}_{CO}$ matrix elements, the output file reports the eigenvalues of $\mathbf{F}_{CO}$ and the various ${}^*\mathbf{F}_{CO}$ matrices in the form of the calculated $\tilde{\nu}_{CO}$ and ${}^*\tilde{\nu}_{CO}$ data, along with the eigenvector matrices **N** and ***N**, which, apart from diagonalizing $\mathbf{F}_{CO}$ and ${}^*\mathbf{F}_{CO}$, connect the internal CO stretching coordinates with the normal coordinates Q, $\mathbf{r} = \mathbf{NQ}$ and ${}^*\mathbf{r} = {}^*\mathbf{N}{}^*\mathbf{Q}$. The program is available on request from B.W.

(61) tom Dieck, H.; Mack, T.; Peters, K.; von Schnering, H.-G. *Z. Naturforsch., B* **1983**, *38*, 568−579.
(62) Schenk, W. A.; Müller, H. *Chem. Ber.* **1982**, *115*, 3618−3630.
(63) Özkar, S.; Kreiter, C. G. *J. Organomet. Chem.* **1986**, *303*, 367−374.
(64) Darensbourg, D. J.; Zalewski, D. J.; Plepys, C.; Campana, C. *Inorg. Chem.* **1987**, *26*, 3727−3732.
(65) Wink, D. J.; Oh, C. K. *Organometallics* **1990**, *9*, 2403−2406.
(66) Grevels, F.-W.; Jacke, J.; Klotzbücher, W. E.; Schaffner, K.; Hooker, R. H.; Rest, A. J. *J. Organomet. Chem.* **1990**, *382*, 201−224.
(67) Berke, H.; Sontag, C. *Z. Naturforsch., B* **1985**, *40*, 794−798.

Table 1. CO Stretching Vibrational Data of $W(CO)_4$(iprop-dab) (1), $Mo(CO)_4$(iprop-dab) (2), $W(CO)_3$(iprop-dab)(η^2-eco) (3), and ^{13}CO-Labeled Isotopomers[53] in Cyclohexane

compd	band position (cm^{-1}) obsd (calcd)	ν(CO) normal coords[a] and EFFF params (N m^{-1})
1 (C_{2v})	A_1 2016.7 (2016.4)	$Q_1(A_1) = 0.3665(r_1 + r_2) +$
	B_1 1918.9[b] (1918.7)	$0.6047(r_3 + r_4)$
	A_1 1914.6[b] (1914.6)	$Q_2(B_1) = -0.7071(r_3 - r_4)$
	B_2 1872.5 (1872.3)	$Q_3(A_1) = -0.6047(r_1 + r_2) +$
1-*1a* (C_s)	A′ 2003.8 (2003.9)	$0.3665(r_3 + r_4)$
	A′ 1915.4[b] (1915.6)	$Q_4(B_2) = 0.7071(r_1 - r_2)$
	A′ 1886.6 (1886.7)	k(ax) = 1543.1
	A″ 1872.6 (1872.3)	k(eq) = 1470.2
1-*1e* (C_s)	A′ 2011.7 (2011.8)	k(ax,ax) = 56.0
	A″ 1918.6[b] (1918.7)	k(eq,eq) = 54.1
	A′ 1905.0 (1904.8)	k(ax,eq) = 35.8
	A′ 1843.6 (1844.2)	
2 (C_{2v})	A_1 2019.3 (2019.0)	$Q_1(A_1) = 0.3433(r_1 + r_2) +$
	B_1 1923.8 (1923.8)	$0.6182(r_3 + r_4)$
	A_1 1914.9 (1914.9)	$Q_2(B_1) = -0.7071(r_3 - r_4)$
	B_2 1871.5 (1871.3)	$Q_3(A_1) = -0.6182(r_1 + r_2) +$
2-*1a* (C_s)	A′ 2005.9 (2006.0)	$0.3433(r_3 + r_4)$
	A′ 1917.2 (1917.0)	$Q_4(B_2) = 0.7071(r_1 - r_2)$
	A′ 1891.0 (1891.0)	k(ax) = 1551.4
	A″ 1871.5 (1871.3)	k(eq) = 1467.4
2-*1e* (C_s)	A′ 2014.8 (2015.0)	k(ax,ax) = 56.4
	A″ 1923.7 (1923.8)	k(eq,eq) = 52.8
	A′ 1904.4 (1904.6)	k(ax,eq) = 35.1
	A′ 1842.8 (1843.2)	
3 (app C_s)	A′ 1963.0 (1962.5)	$Q_1(A') = 0.5135(r_1 + r_2) +$
	A′ 1899.2 (1898.9)	$0.6874r_3$
	A″ 1859.4 (1859.9)	$Q_2(A') = 0.4861(r_1 + r_2) -$
		$0.7262r_3$
		$Q_3(A'') = 0.7071(r_1 - r_2)$
3-*1e′/e″* (C_1)	1954 (1954.3)	k(ax) = 1503.5
	1892 (1892.2)	k(eq′) = k(eq″) = 1453.1
	1833 (1832.6)	k(eq′,eq″) = 55.8
3-*1a* (app C_s)	A′ 1948 (1948.3)	k(ax,eq′) = k(ax,eq″) = 35.0
	A′ 1870 (1870.2)	
	A″ 1860 (1859.9)	

[a] CO internal coordinates r_1 and r_2 represent the equatorial CO groups (cis to each other and trans to the iprop-dab ligand), while r_3 and r_4 represent the axial CO groups. [b] Position located by means of computer-assisted curve fitting.[54]

feature was previously found in a series of *cis*-$M(CO)_2$(N−N)-*trans*-(η^2-olefin)$_2$[35−37,68] and *cis*-$M(CO)_2$(N−N)-*trans*-(η^2-olefin)(η^2-C_{60})[69] complexes. Therefore, **A** and **C** seem more likely than the staggered arrangements **B** and **D**, which have no such precedents. The eclipsed geometry has indeed been verified for the structure of **3** in the crystal by means of X-ray diffraction techniques (vide infra).

The ^{13}C NMR spectra of both **3** and **4** (Table 2) exhibit three lines in the CO region and eight signals for the iprop-dab ligand, one for each carbon atom, while only four resonances are observed for the eight carbon atoms of the η^2-eco ligand. Accordingly, the ^{1}H NMR spectrum of **3** shows two septets for the two methine protons and four doublets for the four methyl groups of the two isopropyl units of the iprop-dab ligand but only one multiplet signal for the two olefinic protons and six multiplets for the 12 aliphatic protons of the η^2-eco ligand. This, for one thing, reflects the reduction in symmetry of the *fac*-$M(CO)_3$(iprop-dab) unit from C_s to C_1 upon attachment of the η^2-eco ligand with its C_2 axis

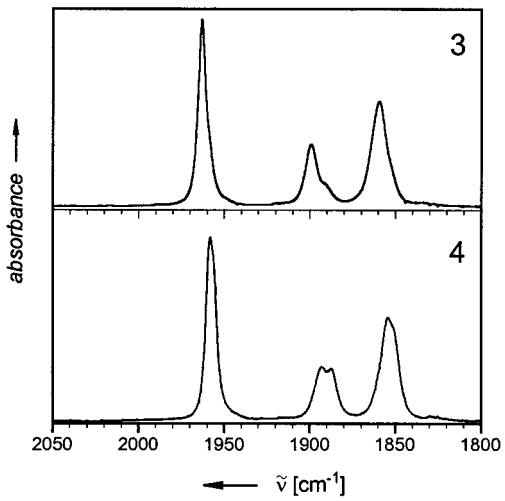

Figure 1. CO stretching vibrational IR bands of $W(CO)_3$(iprop-dab)(η^2-eco) (**3**; 1963.0, 1899.2, and 1859.4 cm^{-1}; in cyclohexane) and $Mo(CO)_3$(iprop-dab)(η^2-eco) (**4**; 1958.0, ∼1956 (sh), 1893.4, 1886.4, 1854.7, and ∼1850 (sh) cm^{-1}; in *n*-hexane containing 5% (*E*)-cyclooctene).

Scheme 3

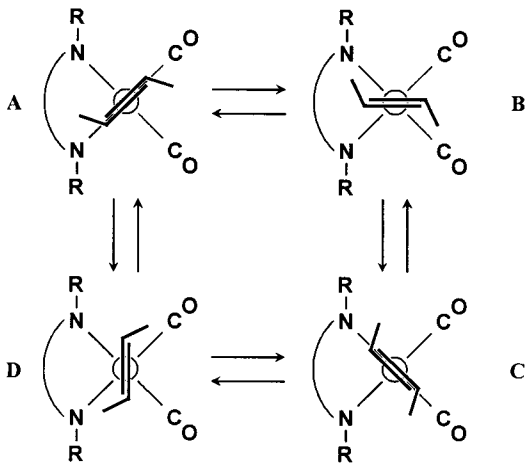

as the only symmetry element. Moreover, it indicates that rotation about the metal−olefin bond axis is a rapid process on the NMR time scale, which not only equilibrates the halves of the η^2-eco ligand but also interconverts the various species shown in Scheme 3.

The chemical shift of the olefinic carbon atoms in **3** (δ 81.96, $\Delta\delta$ = 51.93 ppm) compares well with the data reported for the olefin ligand in $W(CO)_5$(η^2-eco) (δ 83.9, $\Delta\delta$ = 50.0 ppm)[48] and *cis*-$W(CO)_4$(η^2-eco)$_2$ (δ 81.63/86.69, $\Delta\delta$ = 52.26/47.2 ppm),[48] which further substantiates the location of the olefin in a position trans to a carbonyl ligand. In view of their small separation, the two ^{13}C carbonyl resonances at lower field (**3**, δ 223.86 and 224.10; **4**, δ 228.63 and 230.78) are attributed to the two CO groups in the equatorial positions, leaving the one at higher field (**3**, δ 213.16; **4**, δ 216.42) for the single axial CO group. This is in accord with the previously reported ordering of signals associated with the axial and equatorial CO groups in $M(CO)_4$(α-diimine) complexes, δ(CO-eq) > δ(CO-ax).[70]

^{13}CO Enrichment and Energy-Factored CO Force Field Data of 3. Quantitative treatment of the CO

(68) Lai, C.-H.; Cheng, C.-H.; Cheng, M.-C.; Peng, S.-M. *J. Chin. Chem. Soc.* **1993**, *40*, 445−450.

(69) Tang, K.; Zheng, S.; Jin, X.; Zeng, H.; Gu, Z.; Zhou, X.; Tang, Y. *J. Chem. Soc., Dalton Trans.* **1997**, 3585−3587.

(70) Majunke, W.; Leibfritz, D.; Mack, T.; tom Dieck, H. *Chem. Ber.* **1975**, *108*, 3025−3029.

Table 2. ^{13}C NMR Data of M(CO)$_4$(iprop-dab) (1, 2), M(CO)$_3$(η^2-eco)(iprop-dab) (3, 4), and the Free Ligands iprop-dab and eco in Toluene-d_8 at 300 K (δ/ppm ($^1J_{CH}$/Hz))

	iprop-dab			eco		
compd	=CH−	>CH−	−CH$_3$	=CH−	−CH$_2$−	CO
1 (M = W)	157.21 (174)	67.04 (138)	24.79 (127)			207.47 [143][c]
	159.13[a]	66.55[a]	23.98[a]			196.71 (ax-CO)[a,b]
						216.23 (eq-CO)[a,b]
2 (M = Mo)	155.91	66.24	24.16			203.00 (ax-CO)
						223.92 (eq-CO)
3 (M = W)	150.62 (171)	63.49 (141)	22.47 (126)	81.96 (151)	29.44 (125)	213.16 (ax) [149][c]
	151.66 (171)	66.25 (139)	24.25 (128)	[10][c]	37.36 (126)	{∼5}[d]
			25.18 (127)		37.46 (129)	223.86 (eq″) [150][c]
			26.78 (127)			224.10 (eq′) [147][c]
4 (M = Mo)[e]	151.64	63.71	23.19	91.51	29.44	216.42 (ax)
	151.68	65.88	24.02		36.76	228.63 (eq″)
			24.69		37.34	230.78 (eq′)
			25.50			
iprop-dab	159.62 (161)	61.53(133)	23.97(126)			
eco				133.89	29.47 (t,125)	
				(d,151)	35.89 (t,127)	
					36.04 (t,127)	

[a] Data in CD_2Cl_2 at −80 °C. [b] Assignment adapted from ref 70. [c] $^1J(^{13}C-^{183}W)$ from satellite lines. [d] $^2J(^{13}C-^{13}C)$ from multiplets observed in ^{13}CO-enriched samples. [e] In toluene containing 6% (*E*)-cyclooctene.

stretching vibrations of **3** (Figure 1, top), aiming at the characterization of the individual carbonyl ligands in terms of force and interaction constants at the level of the energy-factored CO force field approximation,[55−58] requires additional frequency data from ^{13}CO-enriched samples. Such data have been gathered from samples generated either by photoinitiated CO/^{13}CO exchange of **3** or via a two-step procedure involving thermal conversion of **3** into W(CO)$_3$(^{13}CO)(iprop-dab) (**1-*1***) (Scheme 2) followed by photolysis in the presence of (*E*)-cyclooctene (vide infra).

The first method, photolysis of **3** in the presence of ^{13}CO, can be used to generate ^{13}CO-enriched samples (**3-#**)[53] containing the whole series of W(CO)$_{3-n}$(^{13}CO)$_n$-(iprop-dab)(η^2-eco) species (n = 0−3). As a typical example, MS analysis after ca. 75% conversion of **3** upon irradiation under a ^{13}CO atmosphere (as monitored by IR spectroscopy) shows the presence of **3** (25 ± 5%), **3-*1*** (36 ± 6%), **3-*2*** (30 ± 6%), and **3-*3*** (9 ± 5%).[53] The ^{13}C NMR spectrum is identical with that of unlabeled **3**, apart from a substantial enhancement of the carbonyl resonances, which now appear with clearly recognizable satellite lines arising from coupling to ^{183}W (see Table 2). Moreover, one of these signals (ax-^{13}CO at δ 213.16) exhibits a well-resolved multiplet structure (superimposed triplet and doublet, $J \approx 4.5$ Hz) due to ^{13}C−^{13}C coupling across the metal center, thereby confirming the presence of the doubly and triply ^{13}CO labeled isotopomers. The IR spectrum shows a multitude of closely spaced and overlapping absorptions in the ν(CO) region, which makes it difficult to disentangle the patterns associated with the various positional isotopomers.

Clearer information in this respect is obtained if the irradiation is stopped after low to moderate ^{13}CO enrichment of **3**. The ^{13}C NMR spectra of such samples reveal that photoinitiated incorporation of ^{13}CO from the bulk solution occurs selectively in the equatorial carbonyl positions, one of which (arbitrarily denoted as eq′) is, however, significantly preferred over the other (eq″). After 23% conversion of **3**, for example, the carbonyl region shows three singlets at δ 224.10, 223.86, and 213.15 (cf. Table 2) along with a doublet centered at δ 213.15 in ca. 13:6:1:2 intensity ratio. These data indicate that the equatorially ^{13}CO labeled isotopomers[53] **3-*1e′*** and **3-*1e″*** are generated from **3** in ca. 2.5:1 ratio, while the amount of **3-*1a*** remains at the level of natural abundance. The doublet at δ 213.15 is logically attributed to a minor amount of doubly labeled species carrying one ^{13}CO group in the axial position and another one in an equatorial position (**3-*2ae′*/3-*2ae″***; $^2J(^{13}C-^{13}C) \approx 4.5$ Hz; the corresponding doublets expected at δ 224.10 and 223.86, respectively, are not discernible due to superposition with the aforementioned intense singlets of **3-*1e′*** and **3-*1e″***). Hence, it is clear that ^{13}CO enrichment in the axial position does not take place directly from the bulk solution but occurs via an equatorial position along with incorporation of a second ^{13}CO, as shown in Scheme 4. It is worth emphasizing that the above **3-*1e′*/3-*1e″*/3-*1a*** ratio persists for many hours at ambient temperature, and even after 1 week the system is still far away from equimolar concentrations of the three positional isotopomers. This rigidity is in striking contrast to the fluxional behavior of the tetracarbonyl complex **1**, which, like other compounds of this type,[70] undergoes rapid CO site exchange, as indicated by the appearance of only one single carbonyl resonance in the ^{13}C NMR spectrum (see Table 2).

Scheme 4

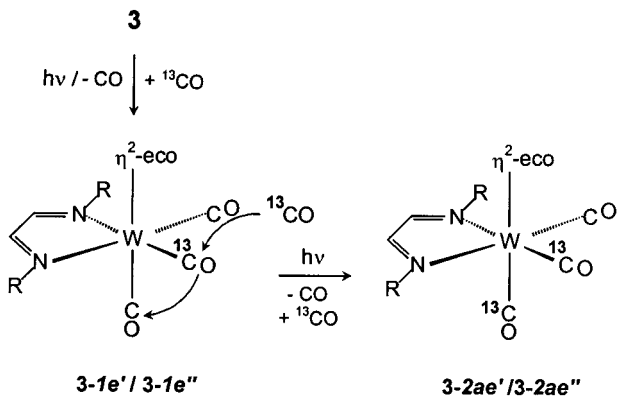

The ν(CO) region in the IR spectrum of the above sample of **3-#** (Figure 2, top) is of course dominated by

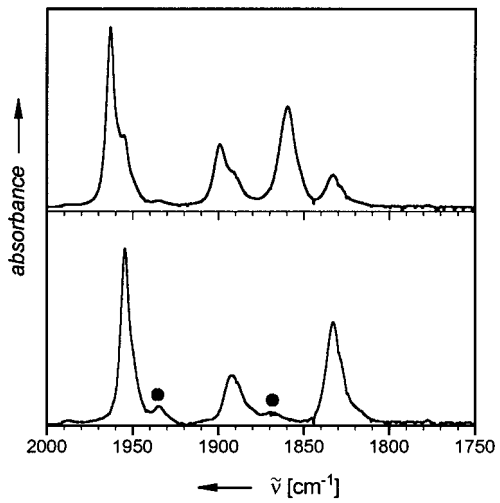

Figure 2. (top) CO stretching vibrational IR spectrum recorded after partial ^{13}CO enrichment of $W(CO)_3$(iprop-dab)(η^2-eco) (**3**; 23% conversion, by IR) in cyclohexane by means of by irradiation under a ^{13}CO atmosphere. (bottom) Corrected spectrum (computer-assisted removal of unreacted **3**; absorbance scale expanded by a factor of 3**)** showing three dominant ν(CO) bands at 1954, 1892, and 1833 cm^{-1}, assigned as $W(CO)_2$(eq′/eq″-^{13}CO)(iprop-dab)-(η^2-eco) (**3-*1e*′**/**3-*1e*″**), along with two minor features at 1935 and 1869 cm^{-1} (●), attributed to the doubly labeled species W(CO)(ax-^{13}CO)(eq′/eq″-^{13}CO)(iprop-dab)(η^2-eco).

the strong absorptions of unreacted **3**. Computer-assisted subtraction of these bands essentially leaves behind a single three-band ν(CO) pattern (Figure 2, bottom), which represents the ca. 2.5:1 mixture of the two monolabeled isotopomers **3-*1e*′** and **3-*1e*″**. The weak features marked with a solid circle (●) can be attributed to the minor amount of doubly labeled species, **3-*2ae*′**/**3-*2ae*″**.

Photolysis of $W(CO)_3(^{13}CO)$(iprop-dab) (**1-*1***) in the presence of (*E*)-cyclooctene was intended to yield a mixture of unlabeled **3** and the three positional isotopomers of monolabeled **3-*1*** (Scheme 5) in order to track out, in particular, the missing ν(CO) pattern of the species **3-*1a***. The irradiation was stopped after 85% conversion of **1-*1***, at which point the IR spectrum revealed some changes in the relative intensities of the emerging ν(CO) bands, indicating that continued irradiation had begun to disturb the initial product distribution. The ^{13}C NMR spectrum, identical with that of **3** with respect to the organic ligands (see Table 2), expectedly shows an enormous enhancement of all three

Scheme 5

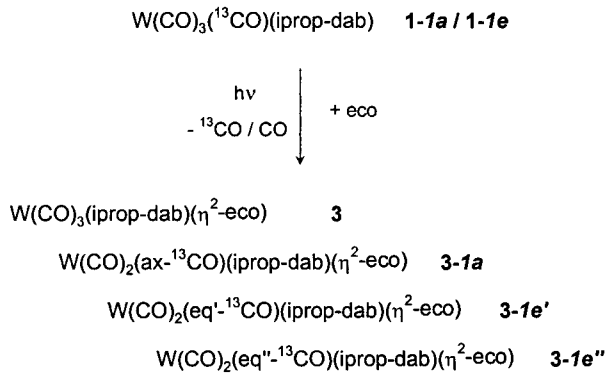

carbonyl resonances. These latter signals essentially appear as singlets (with satellite lines arising from coupling to ^{183}W) with comparable intensities, indicative of a nearly equimolar mixture of the three positional isotopomers, which carry one single ^{13}CO group either in the axial position (**3-*1a***) or in one of the two equatorial positions (**3-*1e*′** and **3-*1e*″**). A weak doublet ($^2J(^{13}C-^{13}C) \approx 5$ Hz), superimposed on the intense singlet associated with **3-*1a***, indicates the presence of doubly labeled **3-*2ae*′**/**3-*2ae*″**, albeit in minor concentration.

The unlabeled component **3**, being silent in the ^{13}C NMR spectrum, clearly shows up in the CO stretching vibrational region of the IR spectrum along with the superimposed bands of the monolabeled isotopomers. Computer-assisted subtraction of the absorptions associated with **3** (1963, 1899, and 1859.5 cm^{-1}; see Figure 1 and Table 1) leaves behind a total number of six dominant and well-resolved bands, which are reasonably grouped, with the help of the Teller−Redlich product rule,[55] into two three-band patterns with approximately 2:1 intensity ratio. The less intense one (1948, 1870, and 1860 cm^{-1}), which was absent in the sample generated by photoinitiated ^{13}CO enrichment (see Figure 2, bottom), is logically assigned to the axially ^{13}CO labeled species **3-*1a***, while the pattern of higher intensity (1954, 1892, and 1833 cm^{-1}) represents the **3-*1e*′**/**3-*1e*″** pair of isotopomers.

These last two species, known from the ^{13}C NMR spectrum to be present in equimolar amounts, are virtually indistinguishable with respect to their carbonyl stretching vibrations. This is tantamount to effective C_s symmetry for the $W(CO)_3$ unit in **3** (i.e., k(eq′) = k(eq″) and k(ax,eq′) = k(ax,eq″); 2 A′ and 1 A″ ν(CO) modes), which is also applicable to **3-*1a*** (the A″ ν(CO) mode of which coincides with that of **3**) but reduces to C_1 in the case of **3-*1e*′**/***e*″**. With these premises, k(ax) = 1503.5 N m^{-1}, k(eq′) = k(eq″) = 1453.1 N m^{-1}, k(ax,eq′) = k(ax,eq″) = 35.0 N m^{-1}, and k(eq′,eq″) = 55.8 N m^{-1} have been evaluated[60] from the frequency data of **3**, **3-*1e*′**/***e*″**, and **3-*1a*** (Table 1). Comparison with the data of the tetracarbonyl complex **1** (Table 1) shows a significant decrease in the principal CO force constants upon replacement of one CO by the olefin ligand, with a more pronounced effect on the axial CO group (Δk(ax) = 39.6 N m^{-1}) than on those in the equatorial positions (Δk(eq) = 17.1 N m^{-1}). This result is consistent with estimates based on tabulated values for the so-called ligand effect constants associated with CO and an olefin ligand (data available for ethene, but not specifically for (*E*)-cyclooctene).[71]

As regards the vibrational equivalency of the two equatorial CO groups (k(eq′) = k(eq″), Table 1), it seems difficult to reconcile this finding with the proposed structure of **3** (**A** and/or **C** in Scheme 3), where the C=C bond of the olefin is in an eclipsed orientation to one of the N−M−CO axes. The crucial point is the single-face π-acceptor character of the olefin ligand, which, in this arrangement, should give rise to discrimination between the two equatorial CO groups with respect to competitive demand for π back-donation from the metal and, thus, should affect the respective CO force constants to different extents. In $W(CO)_5(\eta^2$-eco),[48] for example, the

(71) Timney, J. A. *Inorg. Chem.* **1979**, *9*, 2502−2506.

force constants of the two pairs of equatorial CO groups, eclipsed and orthogonal to the olefin, differ by ca. 20 N m^{-1}.[72] Hence, one might be tempted to discard the notion of an eclipsed structure in favor of the staggered arrangement (**B** and/or **D** in Scheme 3), where the discrimination between the two equatorial CO groups would vanish. However, this consideration was disproved by the single-crystal X-ray structure analysis of **3**.

Structure of W(CO)$_3$(iprop-dab)(η^2-eco) (3) in the Crystal. The results of the single-crystal X-ray structure analysis of **3** are summarized in Figure 3, which shows a view along a face diagonal of the essentially octahedrally coordinated W atom. The major distortion from ideal octahedral geometry originates from the iprop-dab ligand, which makes a N1−W−N2 angle of 72.6(3)° at the metal. This value lies at the smaller end of the range of observed angles in transition-metal complexes containing this ligand (72−87°)[61,73] and is probably a consequence of the relatively long N−W distances (mean N−W = 2.19(2) Å). The ligand is end-on coordinated to the W atom via the N atoms and coplanar with the two CO groups in trans positions (rms deviation from the mean plane through N1, C12, C13, N2, C2, O2, C3, O3, and W: 0.06 Å).

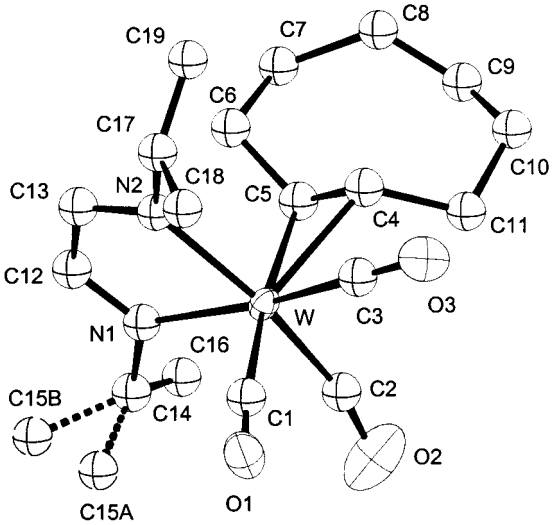

Figure 3. Structure of *fac*-W(CO)$_3$(iprop-dab)(η^2-eco) (**3**) in the crystal state. Hydrogen atoms have been omitted for clarity. One methyl group is disordered (50:50) over two positions (C15A, C15B). Selected distances (Å) and angles (deg) (C$_{mp}$ is the midpoint of the bond C4−C5): W−C4 = 2.402(8), W−C5 = 2.406(8), W−C1 = 1.973(7), W−C2 = 1.95(2), W−C3 = 1.99(2), W−N1 = 2.19(1), W−N2 = 2.18(1), C4−C5 = 1.35(1), C4−C11 = 1.53(1), C5−C6 = 1.52(1); N1−W−N2 = 72.6(3), N1−W−C$_{mp}$ = 95.0(6), N1−W−C1 = 103.3(4), N1−W−C2 = 95.8(5), N1−W−C3 = 169.5(5), N2−W−C$_{mp}$ = 94.4(5), N2−W−C1 = 95.0(4), N2−W−C2 = 168.4(5), N2−W−C3 = 97.5(5), C1−W−C4 = 145.4(3), C1−W−C5 = 173.7(3), C$_{mp}$−W−C1 = 161.2(5), C$_{mp}$−W−C2 = 85.9(5), C$_{mp}$−W−C3 = 89.0(6), C1−W−C2 = 88.2(5), C1−W−C3 = 73.6(5), C2−W−C3 = 94.1(4).

As suggested by structure **A** in Scheme 3, the η^2-eco ligand takes up a position cis to the two N atoms, with its C=C bond axis (C4−C5) lying eclipsed to one of the N−W−CO axes (rms deviation from the mean plane through C4, C5, N1, W, C3, and O3: 0.06 Å). Such an eclipsed arrangement, theoretically predicted for group 6 M(CO)$_5$(η^2-ethene) and *trans*-M(CO)$_4$(η^2-ethene)$_2$ complexes,[74−76] has been observed with a wide range of olefin-substituted group 6 metal carbonyls[40,42,45,48,77,78] and related compounds[35−38,68,69,79,80] containing nitrogen or phosphorus ligands in addition to CO and the olefin. The distances of the W atom to the C atoms of the olefinic double bond (W−C4 = 2.402(8) Å, W−C5 = 2.406(8) Å) are comparable with those in the related compound W(CO)$_5$(η^2-eco) (mean W−C = 2.44(2) Å)[48] and slightly shorter than in W(CO)$_5$(η^2-(*Z*)-cyclooctene) (mean W−C = 2.50(2) Å),[78] though hardly significantly so.

It is worth noting that the carbonyl group C1−O1 does not lie exactly in a position trans to the midpoint of the C=C double bond of the olefin ligand (C$_{mp}$−W−C1 = 161.2(5)°), as found for W(CO)$_5$(η^2-eco) (C$_{mp}$−W−C(O) = 177°).[48] Rather, it is bent away from the iprop-dab ligand (N1−W−C1 = 103.3(4)°) toward the carbonyl group C3−O3 (C3−W−C1 = 73.6(5)°). This distortion occurs almost in the direction of the plane defined by N1, C4, C5, C3, O3, and W but appears to have no effect on the W−C distances to C4 and C5, which are identical within experimental error. Crystal packing or intramolecular steric repulsion is unlikely to be responsible for this contortion, since there are no intra- or intermolecular distances less than 3.1 Å involving O1 and non-H atoms. Lacking a more substantiated explanation, we suspect that the substantial deviation of C$_{mp}$−W−C1 from linearity in some way cancels the anticipated discriminative influence of η^2-olefin on the two equatorial CO groups.

Table 3. UV−vis Absorption Data (λ_{max}/nm (ϵ/L mol^{-1} cm^{-1})) of M(CO)$_4$(iprop-dab) (1, M = W; 2, M = Mo) and *fac*-M(CO)$_3$(iprop-dab)(η^2-eco) (3, M = W; 4, M = Mo) in Cyclohexane Containing 15 mM (*E*)-Cyclooctene

M = W		M = Mo	
1	**3**	**2**	**4**
	∼650 (1930)		∼690 (1480)
549 (16 600)		562 (15 000)	
	520 (10 200)		558 (9100)
365 (2010)		371 (2560)	
	∼385 (960)		∼385 (860)
	333 (4920)		338 (4500)
	302 (6160)		301 (5330)
291 (7230)		291 (9800)	

Electronic Absorption Spectra and Quantum Yields. The UV−vis absorption spectra of the M(CO)$_4$(iprop-dab) complexes **1** (M = W) and **2** (M = Mo), as displayed in Figure 4 and summarized in Table 3, reproduce very well the previously reported

(72) Grevels, F.-W., Unpublished material.
(73) Hessen, B.; Bol, J. E.; de Boer, J. L.; Meetsma, A.; Teuben, J. H. *J. Chem. Soc., Chem. Commun.* **1989**, 1276−1277.
(74) Bachmann, C.; Demuynck, J.; Veillard, A. *J. Am. Chem. Soc.* **1978**, *100*, 2366−2369.
(75) Albright, T. A.; Hoffmann, R.; Thibeault, J. C.; Thorn, D. L. *J. Am. Chem. Soc.* **1979**, *101*, 3801−3812.
(76) Pidun, U.; Frenking, G. *Organometallics* **1995**, *14*, 5325−5336.
(77) Szymańska-Buzar, T.; Kern, K.; Downs, A. J.; Greene, T. M.; Morris, L. J.; Parsons, S. *New J. Chem.* **1999**, *23*, 407−416.
(78) Toma, J. M. D. R.; Toma, P. H.; Fanwick, P. E.; Bergstrom, D. E.; Byrn, S. R. *J. Crystallogr. Spectrosc. Res.* **1993**, *23*, 41−47.
(79) Butts, M. D.; Bryan, J. C.; Luo, X.-L.; Kubas, G. J. *Inorg. Chem.* **1997**, *36*, 3341−3353.
(80) Hsu, H.-F.; Du, Y.; Albrecht-Schmidt, T. E.; Wilson, S. R.; Shapley, J. R. *Organometallics* **1998**, *17*, 1756−1761.

data.[10,11,13,16,81] The spectra exhibit an intense band in the visible region, previously shown to comprise several closely spaced transitions with different polarizations and with varying degrees of charge transfer from the

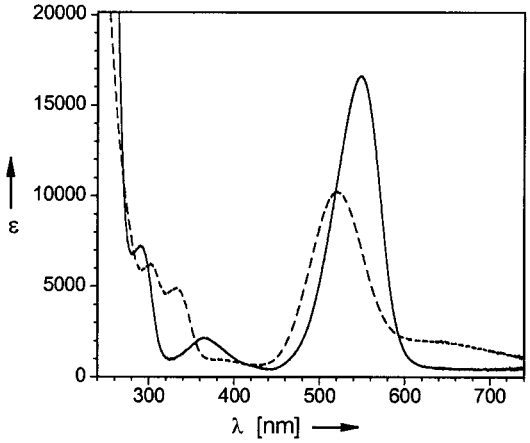

Figure 4. UV−vis absorption spectra of $W(CO)_4$(iprop-dab) (**1**; —) and *fac*-$W(CO)_3$(iprop-dab)(η^2-eco) (**3**; - - -) in cyclohexane containing 15 mM (*E*)-cyclooctene.

metal to the α-diimine ligand (CTML),[10,11,16] in addition to distinctly weaker absorptions at shorter wavelengths, which are reasonably interpreted as ligand field (LF) transitions.[81]

The spectral changes resulting from the substitution of CO by (*E*)-cyclooctene (Figure 4, Table 3) may be used for monitoring the photochemical generation of the *fac*-$M(CO)_3$(iprop-dab)(η^2-eco) complexes **3** and **4** from the respective starting materials **1** and **2** (Scheme 1). However, although the UV−vis reaction spectra exhibit seemingly clean isosbestic points up to nearly complete conversion, comparative examination of the same sample solutions by means of quantitative IR spectroscopy in the CO stretching vibrational region revealed that the intense ν(CO) absorptions with their narrow band shapes and well-separated maxima provide for better control of the material balances and, hence, for more reliable analytical results.

Quantum yields have been determined at several selected wavelengths (Table 4), taking into account mutual internal light filtering,[82] from the combined results of 8−12 individual runs[83] that involve conversions of the respective starting material ranging from 5 to 60%. This is illustrated in Figure 5 for the case of M = Mo. For three different wavelengths of excitation the plots of the measured concentrations $\tilde{c}_2$ and $\tilde{c}_4$ vs the absorbed amount of light (τ)[84] are shown along with the computed functions $\tilde{c}_i = f(\tau)$, which fit satisfactorily to the experimental points. Similar results have been obtained for the analogous conversion of the tungsten complex **1** into *fac*-$W(CO)_3$(iprop-dab)(η^2-eco) (**3**).

Table 4. Quantum Yields[a] for the Photosubstitution of CO in $M(CO)_4$(iprop-dab) (1, M = W; 2, M = Mo; ca. 1 mM in Cyclohexane) by (*E*)-Cyclooctene (ca. 15 mM) with Formation of *fac*-$M(CO)_3$(iprop-dab)(η^2-eco) (3, M = W; 4, M = Mo)

	M = W		M = Mo	
λ_{exc} (nm)	Φ_{13}	ϵ_1/ϵ_3 (L mol^{-1} cm^{-1})	Φ_{24}	ϵ_2/ϵ_4 (L mol^{-1} cm^{-1})
254	0.092	28920/20280		
302	0.074[b]	4930/6160	0.101	6820/5250
	0.080			
	0.079[c]			
365	0.038	2010/1050	0.041	2130/1550
405	0.019	770/760	0.020	610/665
548	∼0.001[d]		∼0.001[d]	

[a] Evaluated, taking into account mutual internal light filtering, from the combined results of 8−12 individual runs. [b] In the presence of 3 mM (*E*)-cyclooctene. [c] In the presence of 100 mM (*E*)-cyclooctene. [d] Conversion 3−10%, internal light filtering negligible.

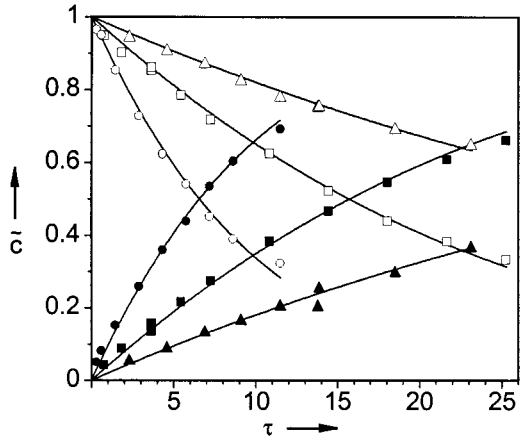

Figure 5. Conversion of $Mo(CO)_4$(iprop-dab) (**2**, open symbols) into $Mo(CO)_3$(iprop-dab)(η^2-eco) (**4**, filled symbols) upon irradiation at 302 nm (○/●; Φ_{24} = 0.101), 365 nm (□/■; Φ_{24} = 0.041), and 405 nm (△/▲; Φ_{24} = 0.020) in cyclohexane containing 15 mM (*E*)-cyclooctene. The symbols indicate the experimental data points, while the curves represent $\tilde{c}_i = f(\tau)$, computed with the evaluated quantum yields and ϵ_i values listed in Table 4.

As a general trend, the quantum yields (Table 4) decrease gradually from ca. 0.1 to 0.02 with increasing wavelength of excitation in the ligand field region and then drop sharply to 0.001 upon irradiation at 548 nm into the dominant visible absorption band. This latter result reflects the notoriously low reactivity of the CTML excited states of group 6 $M(CO)_4$(α-diimine) complexes.[13,23,25] Quantum yields on the order of 10^{-3}−10^{-5} were found, for example, for the photosubstitution of CO in a series of $W(CO)_4$(R-phen) and $W(CO)_4$(R-dab) complexes occurring upon long-wavelength irradiation in the presence of phosphines and other potential ligands.[25] Nucleophilic attack of the entering ligand on the complex in its CTML excited state has been invoked

(81) Schadt, M. J.; Lees, A. J. *Inorg. Chem.* **1986**, *25*, 672−677.
(82) Kling, O.; Nikolaiski, E.; Schläfer, H. L. *Ber. Bunsen-Ges. Phys. Chem.* **1963**, *67*, 883−892.
(83) The evaluation of the quantum yield Φ_{AB} for the photoreaction

$$A \xrightarrow{h\nu} B$$

taking into account mutual internal light filtering, is based on the functional relationship $\Phi_{AB} = (1/\epsilon_A\,\tau)[(\epsilon_A - \epsilon_B)(1 - \tilde{c}_A) - \epsilon_B \ln(\tilde{c}_A)]$ (adapted from ref 82) in combination with the stoichiometric condition $\tilde{c}_B = 1 - \tilde{c}_A$.[84] It has been performed by means of a least-squares fit procedure as follows. Starting with a reasonable guess for Φ_{AB}, the routine ROOT (WURZEL) of the Mathcad software package (MathSoft, Inc., 101 Main Street, Cambridge, MA 02142. *Benutzerhandbuch Mathcad 7 für Profis*; International Thomson: Bonn, Germany, 1997; Chapter 15) is used to solve the above equation numerically for $\tilde{c}_A$ and $\tilde{c}_B$ for each of the experimental values of τ. The routine MINERR (MINFEHL) is used to find that value of Φ_{AB} which gives the best least-squares fit of the computed concentrations to the experimental data. The appropriate program is available on request from B.W.
(84) Following our notation in a previous study,[48] the concentrations of the starting material A and the product B as well as the amount of light absorbed by the system are normalized to the initial concentration of A by setting $\tilde{c}_{A(B)} = c_{A(B)}/c_A{}^0$ and $\tau = (1/c_A{}^0)\int_0^t Q_{abs}\,dt$.

in that detailed study in order to rationalize the influence of the substituents R and the properties of the incoming ligands on the quantum yield.

Such an associative mechanism may also be applicable to the very inefficient reactions of **1** and **2** with (*E*)-cyclooctene occurring upon irradiation at $\lambda_{exc} = 548$ nm, but apparently it does not make a noticeable contribution to the much higher reactivity at shorter wavelengths of excitation. This is demonstrated by the fact that an increase in the (*E*)-cyclooctene concentration from 15 to 100 mM leaves the quantum yield for the conversion of **1** into **3** at $\lambda_{exc} = 302$ nm virtually unchanged (see Table 4). We rather suggest that here a dissociative two-step mechanism is operative, which involves photolytic loss of CO with generation of the (solvated) M(CO)$_3$(iprop-dab) fragment, followed by taking up of (*E*)-cyclooctene to form the *fac*-M(CO)$_3$(iprop-dab)(η^2-eco) product (Scheme 6). Competitive recapturing of the fragment by the photodissociated CO could, in principle, diminish the quantum yield of the overall process. However, this appears to be negligible under the actual conditions of our quantum determinations, i.e., in the presence of 15 mM (*E*)-cyclooctene under an inert atmosphere, since even a drastic reduction of this concentration by a factor of 5 (to 3 mM) has only a minor effect on the quantum yield, as demonstrated at $\lambda_{exc} = 302$ nm for the case of tungsten (see Table 4). Hence, one can take the observed quantum yields as a direct measure of the efficiency of the initial photolytic step in Scheme 6.

Scheme 6

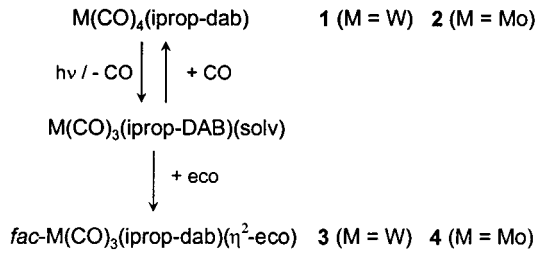

It seems likely that the involvement of different dissociative excited states, with varying probabilities of relaxation to either the ground state or the unreactive CTML excited state(s), is responsible for the wavelength dependence of the quantum yields. However, we are not yet in a position to expatiate on the events occurring on the excited-state surface(s). We rather have focused our efforts on the detection and characterization of the supposed intermediate, the CO loss product M(CO)$_3$(iprop-dab). To this end, the photolytic behavior of Mo(CO)$_4$(iprop-dab) (**2**) was investigated by means of low-temperature matrix isolation techniques as well as flash photolysis at ambient temperature in hydrocarbon solution in combination with time-resolved IR and UV−vis spectroscopy.

Photolysis of Mo(CO)$_4$(iprop-dab) (2) in Low-Temperature Matrixes. Both the IR ν(CO) and UV−vis absorptions of **2** (and its isotopically substituted derivatives **2-*1a*/2-*1e***) in solid argon at 10 K (Table 5) closely resemble the respective spectra in hydrocarbon solution at ambient temperature (Tables 1 and 3).

Photolysis of **2** in the argon matrix leads to IR spectral changes in the CO stretching vibrational region (Figure

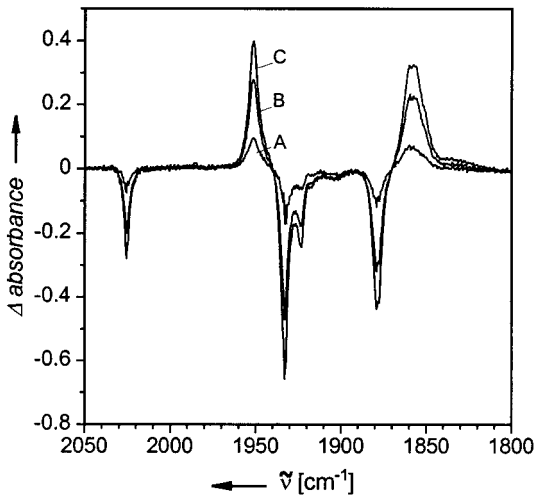

Figure 6. CO stretching vibrational difference spectra illustrating the conversion of Mo(CO)$_4$(iprop-dab) (**2**) into *fac*-Mo(CO)$_3$(iprop-dab) (**5**) upon irradiation in solid argon at 10 K for 5 min at 313 nm (A), followed by further photolysis at 289 nm for two consecutive periods of 1 min each (B, C, 50% conversion of **2**).

Scheme 7

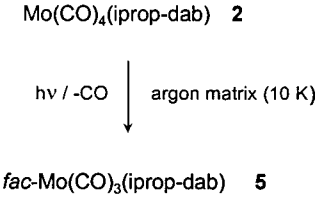

6) which along with the appearance of a feature, albeit weak, at 2138 cm^{-1} (not shown in Figure 6) indicate the occurrence of one single reaction involving loss of CO with formation of a fragment assigned (vide infra) as *fac*-Mo(CO)$_3$(iprop-dab) (**5**) (Scheme 7). The efficiency of this process shows a wavelength dependence similar to that observed for the conversion of **2** into the olefin-substituted product **4** (Table 4). Thus, long-wavelength irradiation through a 550 or 400 nm cutoff filter into the CTML band of **2** has no noticeable effect, even after extended periods of 30−45 min. At higher energies of excitation, the first IR spectral changes are just recognizable after irradiation at $\lambda_{exc} = 365$ or 334 nm into the weak LF absorption of **2** around 360 nm. As illustrated by the sequence of difference spectra in Figure 6, the photolysis becomes more and more effective at $\lambda_{exc} = 313$ and 289 nm: i.e., upon approaching the electronic absorption of **2** centered at 285 nm.

Close inspection of the difference spectra displayed in Figure 6 shows that the depletion bands reproduce the ν(CO) pattern of **2** in every respect, thus excluding any disturbing overlap with the product absorptions emerging at 1950.5 and 1857.3 cm^{-1}. This latter pattern, with a narrow and intense high-frequency band and a somewhat broader absorption at lower frequency, rules out a *mer*-M(CO)$_3$ skeleton, which would exhibit a much weaker absorption at the highest frequency position.[55] It rather indicates a structure with a *fac*-M(CO)$_3$ unit, commonly characterized by three ν(CO) bands with comparable intensities (e.g., 2 A′ and A″ under C_s symmetry), unless 3-fold rotational symmetry renders two of them degenerate (A_1 and E under C_{3v} symmetry).

Table 5. IR ν(CO) and UV−Vis Spectral Data of Mo(CO)$_4$(iprop-dab) (2) and Related Compounds in Low-Temperature Matrices at 10 K

compd	matrix	$\tilde{\nu}$(CO) (cm^{-1}) obsd (calcd)				CO force field data (N m^{-1})	UV−vis λ_{max} (nm)
2 (C_{2v})	Ar	2025 (A_1, 2024.4)	1932 (B_1, 1932.0)	1922 (A_1, 1921.7)	1877 (B_2, 1876.7)	k_{ax} = 1563.4, k_{eq} = 1475.6, $k_{ax,ax}$ = 55.6, $k_{eq,eq}$ = 52.8, $k_{ax,eq}$ = 34.0	552 (vst), ∼510 (sh), 360 (w), 285 (m)
2-*1a* (C_s)	Ar	2011 (A′, 2011.1)	1924 (A′, 1924.2)	1899 (A′, 1898.9)	1877 (A″, 1876.7)		
2-*1e* (C_s)	Ar	2020 (A′, 2020.5)	1932 (A″, 1932.0)	1911 (A′, 1911.1)	1848 (A′, 1848.6)		553 (vst), ∼510 (sh), 360 (w), 285 (m)
2 (C_{2v})	Ar:CO (3:1)	2021.5 (A_1)	1925 (B_1)	1911.5 (A_1)	1866 (B_2)		536 (vst), ∼495 (sh), 368 (w), 290 (m)
2 (C_{2v})	Ar:^{13}CO (3:1)	2021 (A_1, 2021.0)	1924 (B_1, 1923.4)	1911.5 (A_1, 1910.7)	1865 (B_2, 1864.3)	k_{ax} = 1552.7, k_{eq} = 1458.8, $k_{ax,ax}$ = 58.3, $k_{eq,eq}$ = 54.9, $k_{ax,eq}$ = 36.4	529 (vst), ∼491 (sh), 371 (w), 291 (m)
2-*1a* (C_s)	Ar:^{13}CO (3:1)	2007.5 (A′, 2007.5)	1913 (A′, 1914.0)	1889.5 (A′, 1889.9)	1863.5 (A″, 1864.3)		
2-*1e* (C_s)	Ar:^{13}CO (3:1)	(A′, 2017.1)	(A″, 1923.4)	(A′, 1900.0)	(A′, 1836.5)		
2 (C_{2v})	N_2	2023.5 (A_1, 2023.6)	1927.5 (B_1, 1927.3)	1917.2 (A_1, 1917.3)	1874.5 (B_2, 1874.3)	k_{ax} = 1557.8, k_{eq} = 1471.1, $k_{ax,ax}$ = 57.2, $k_{eq,eq}$ = 52.6, $k_{ax,eq}$ = 35.7	540 (vst), ∼500 (sh), 365 (w), 286 (m)
2-*1a* (C_s)	N_2	2010.7 (A′, 2010.4)	[∼1920][a] (A′, 1919.8)	1894.6 (A′, 1894.3)	1874.9 (A″, 1874.3)		
2-*1e* (C_s)	N_2	2019.4 (A′, 2019.6)	1927.0 (A″, 1927.3)	1907.2 (A′, 1907.0)	1845.1 (A′, 1846.1)		542 (vst), ∼500 (sh), ∼370 (sh), 294 (m)
5[b]) (eff C_{3v})	Ar	1950.5 (A_1, 1950.5)	1857.3 (br) (E, 1857.4)			k_{CO} = 1441.4, $k_{CO,CO}$ = 47.8	673 (vst)
5-*1* (eff C_s)	Ar	1939.7 (A′, 1939.7)	1858.3 (A″, 1857.4)	1825.3 (A′, 1826.1)			674 (vst), 306 (m, sh)
5 (eff C_{3v})	Ar:CO (3:1)	1943 (A_1)	1842 (E)				658 (vst)
5 (eff C_{3v})	Ar/^{13}CO (3:1)	1940 (A_1)	1841 (E)				650 (vst)
6[c] (C_s)	N_2	1956.0 (A′, 1956.0), 2208 ν(N≡N)	1885.1 (A′, 1885.2)	1857.3 (A″, 1857.2)		k_{ax} = 1475.4, k_{eq} = 1449.5, $k_{eq,eq}$ = 56.3, $k_{ax,eq}$ = 37.3 st	590 (st)
6-*1a* (C_s)	N_2	[∼1946][a] (A′, 1945.1), 2208 ν(N≡N)	[∼1858][a] (A″, 1857.2)	[∼1858][a] (A′, 1853.5)			
6-*1e* (C_1)	N_2	[∼1946][a] (1945.8), 2208 ν(N≡N)	1880.8 (1880.7)	1829.5 (1829.7)			

[a] The accuracy of observed frequencies (given in square brackets) suffers from overlap with other bands, and therefore, these data were not included in the EFFF calculation. [b] CO normal coordinates: $Q_1(A_1) = 0.5774(r_1 + r_2 + r_3)$; $Q_2(E_x) = 0.4082(r_1 + r_2) - 0.8165r_3$; $Q_3(E_y) = 0.7071(r_1 - r_2)$; note that r_3 is positioned on the x axis. [c] CO normal coordinates: $Q_1(A') = 0.5649(r_1 + r_2) + 0.6014r_3$; $Q_2(A') = -0.4253(r_1 + r_2) + 0.7989r_3$; $Q_3(A'') = 0.7071(r_1 - r_2)$.

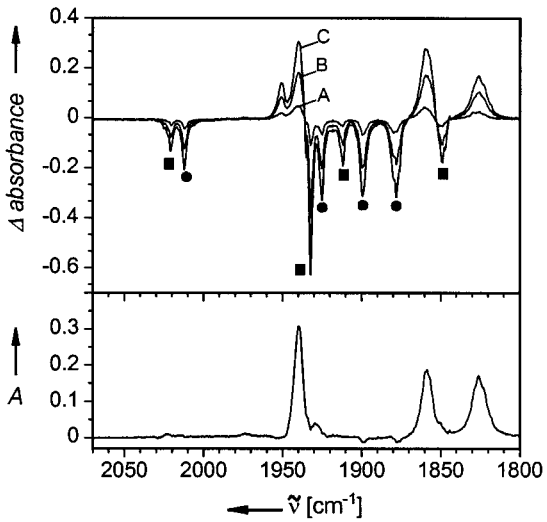

Figure 7. (top) CO stretching vibrational difference spectra illustrating the conversion of Mo(CO)$_3$(^{13}CO)(iprop-dab) (**2-*1a*** (●) and **2-*1e*** (■)) into the *fac*-Mo(CO)$_3$(iprop-dab) (**5**) and *fac*-Mo(CO)$_2$(^{13}CO)(iprop-dab) (**5-*1***) fragments upon irradiation in solid argon at 10 K for 30 min at 313 nm (A), followed by further photolysis at 289 nm for two consecutive periods of 3 min (B) and 15 min (C, 85% conversion), respectively. (bottom) ν(CO) pattern of *fac*-Mo(CO)$_2$(^{13}CO)(iprop-dab) (**5-*1***), obtained from the above difference spectrum by computer-assisted removal of the depletion bands, followed by subtraction of the absorptions associated with **5**.

Hence, we identify the CO loss photoproduct of **2** as the *fac*-M(CO)$_3$(iprop-dab) (**5**) fragment, which is further characterized by complementary ν(CO) data of the ^{13}CO-substituted derivative **5-*1*** generated from **2-*1***.

The IR difference spectra recorded upon photolysis of Mo(CO)$_3$(^{13}CO)(iprop-dab) (**2-*1***) under similar conditions (Figure 7, top) expectedly show the simultaneous depletion of both stereoisotopomers, Mo(CO)$_3$(ax-^{13}CO)(iprop-dab) (**2-*1a***) and Mo(CO)$_3$(eq-^{13}CO)(iprop-dab) (**2-*1e***).[53] Concomitantly, four strong product bands emerge at 1950.5, 1939.7, ~1858, and 1825.3 cm^{-1} along with a weak absorption (not shown in Figure 7) at 2138 cm^{-1} and a barely discernible feature at 2091 cm^{-1}. The last two indicate the release of CO and ^{13}CO, respectively, expected to occur in a 3:1 ratio with formation of the ^{13}CO-labeled fragment **5-*1*** and its unlabeled companion **5** (Scheme 8). The iprop-dab ligand imposes C_s symmetry on the Mo(CO)$_3$ unit in **5**, and therefore, **5-*1*** should exist as a 2:1 mixture of stereoisotopomers. However, its ν(CO) spectrum (Figure 7, bottom), obtained from the ultimately recorded difference spectrum (Figure 7C) by means of computer-assisted removal of both the depletion bands of the starting material and the absorptions associated with unlabeled **5**, shows only one single three-band ν(CO) pattern: i.e., the two stereoisotopomers of **5-*1*** are virtually indistinguishable in this respect. This implicitly means that the CO stretching vibrations of this system can be treated as if the Mo(CO)$_3$ unit in **5** possesses 3-fold rotational symmetry (i.e., $k_1 = k_2 = k_3$ and $k_{12} = k_{13} = k_{23}$; 2 ν(CO) modes, denoted A_1 and E under C_{3v}), which reduces to C_s upon introduction of the ^{13}CO label (3 ν(CO) modes: 2 A′, A″, the latter being coincident with the ν(CO) E mode of the unlabeled parent). With these premises, k_{CO} = 1441.4 N m^{-1} and $k_{CO,CO}$ = 47.8 N m^{-1} have been

Scheme 8

Mo(CO)$_3$(^{13}CO)(iprop-dab) **2-*1a* / 2-*1e***

[argon matrix at 10 K]

hν ↓ - CO/^{13}CO

fac-Mo(CO)$_3$(iprop-dab) **5**

fac-Mo(CO)$_2$(^{13}CO)(iprop-dab) **5-*1***

evaluated[60] from the observed frequencies listed in Table 5. This result is in excellent agreement with predictions made on the basis of the so-called ligand effect constants,[71] since, with ϵ_{CO}^{cis} = 33.5 N m^{-1} and ϵ_{CO}^{trans} = 126.1 N m^{-1}, loss of CO from an axial position of **2** should reduce k(ax) from 1563.4 N m^{-1} to 1437.3 N m^{-1} and k(eq) from 1475.6 N m^{-1} to 1442.1 N m^{-1}.

The UV−vis spectrum shows a pronounced bathochromic shift of the CTML electronic absorption band from 553 to 674 nm (Figure 8). The spectra displayed in this figure are taken from an experiment with the isotopically substituted sample **2-*1***, but the same results have of course been obtained with the unlabeled compound **2**. The solid curve shows the UV−vis spectrum of **2-*1*** after deposition in the argon matrix before irradiation, while the dashed curve represents the situation after 85% conversion into **5-*1***. The weak band around 553 nm is therefore entirely due to the absorption of the residual amount of unreacted starting material. Hence it is clear, and worth emphasizing, that the loss of one carbonyl ligand from **2-*1*** (or **2**) affects all transitions contributing to the CTML absorption band to roughly the same extent: i.e., the involved metal d levels are equally destabilized.

The reactions in both Scheme 7 (photodissociation of CO from **2**) and Scheme 8 (photodissociation of CO/^{13}CO from **2-*1a*/2-*1e***) proved photoreversible, albeit with moderate efficiency, upon irradiation into the dominant long-wavelength absorption band of **5** and **5-*1***, respectively (Scheme 9). Thus, after 85% conversion of **2-*1a*/2-*1e*** into **5**/**5-*1*** (Figure 7, top, spectrum C), 22% recovery

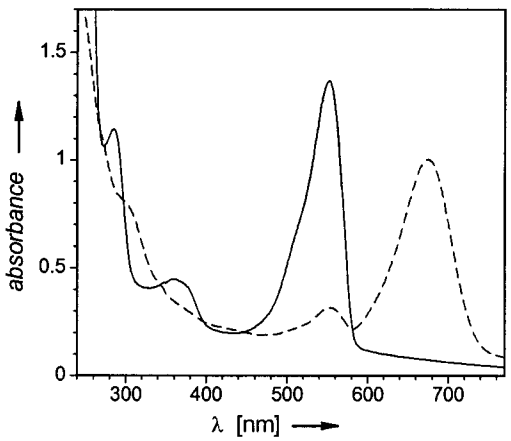

Figure 8. Electronic absorption spectrum of Mo(CO)$_3$(^{13}CO)(iprop-dab) (**2-1**), deposited in solid argon at 10 K, before irradiation (—) and after photoinitiated 85% conversion into Mo(CO)$_3$(iprop-dab)/Mo(CO)$_2$(^{13}CO)(iprop-dab) (**5/5-1**) (- - -). Note that Figure 7 (top, spectrum C) shows the ν(CO) IR spectrum of the same sample.

Scheme 9

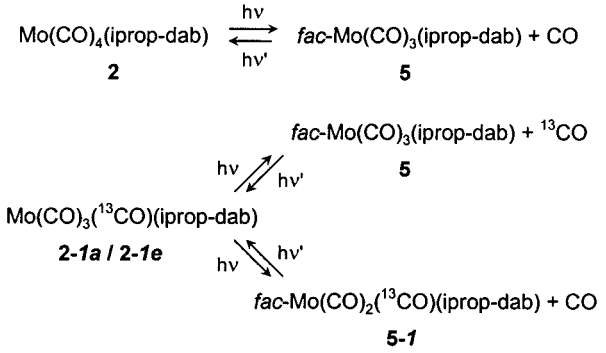

Scheme 10

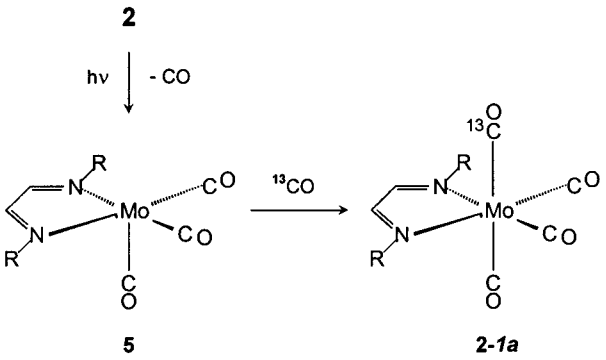

of the starting material was achieved within 5.5 h of irradiation at 670 nm, without any sign of CO/^{13}CO scrambling.

Long-wavelength irradiation of **5** is not essential to the take-up of CO with re-formation of **2**. Rather, this process occurs also under short-wavelength photolysis, concomitantly with the photogeneration of **5**, provided that an excess of added CO is present. Thus, in a CO-doped argon matrix (Ar:CO = 3:1) the conversion of **2** into **5**, as monitored by IR and UV−vis spectroscopy (Table 5), does not exceed 55−60%, even after 2.5 h photolysis at 289 nm. Under these circumstances, subsequent long-wavelength irradiation through a 590 nm cutoff ultimately leads to almost complete recovery of **2**.

The analogous experiment in a ^{13}CO-doped matrix (Ar:^{13}CO = 3:1) reveals that the addition of carbon monoxide from the matrix environment to the tricarbonyl fragment **5** occurs stereospecifically into the vacant axial coordination site (Scheme 10). This is evident from the product ν(CO) spectrum displayed in Figure 9, recorded after 30% conversion of **2** upon brief irradiation (4 min) at 289 nm. It shows, along with the two ν(CO) bands of **5** (marked ■) at 1940 and 1841 cm^{-1}, a four-band pattern (marked ●) emerging at 2007.5, 1913, 1889.5, and 1863.5 cm^{-1} which represents a mono-^{13}CO-substituted derivative of **2**, Mo(CO)$_3$(^{13}CO)(iprop-dab) (**2-*1***), as verified by the Teller−Redlich product rule.[55] One of these bands (1863.5 cm^{-1}) coincides, within experimental error, with the B_2 ν(CO) mode of **2** (1865 cm^{-1}, Table 5), and this identifies the observed species as the axially labeled isotopomer *fac*-Mo(CO)$_3$(ax-^{13}CO)(iprop-dab) (**2-*1a***). The combined frequency data of **2** and **2-*1a*** were used to evaluate the CO force field parameters (Table 5) and, moreover, to calculate the frequencies of the absent isotopomer *mer*-Mo(CO)$_3$(eq-^{13}CO)(iprop-dab) (**2-*1e***). As illustrated in Figure 9, this latter species (positions marked ▼) would clearly be recognizable if it were present.

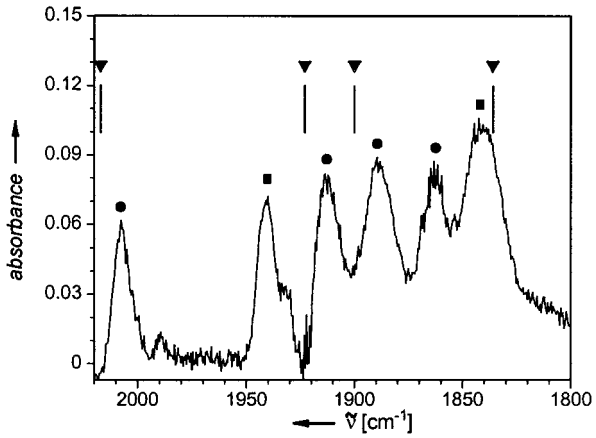

Figure 9. CO stretching vibrational bands of *fac*-Mo(CO)$_3$(iprop-dab) (**5**; ■) and Mo(CO)$_3$(ax-^{13}CO)(iprop-dab) (**2-*1a***; ●) generated from Mo(CO)$_4$(iprop-dab) (**2**) in a Ar/^{13}CO (3:1) matrix as the result of 4 min of photolysis at 289 nm (30% conversion). Note that the absorptions of unreacted **2** have been removed by computer-assisted subtraction; the symbol ▼ indicates the ν(CO) positions of the absent isotopomer Mo(CO)$_3$(eq-^{13}CO)(iprop-dab) (**2-*1e***).

It is worth mentioning that the presence of carbon monoxide apparently makes the matrix a more polar medium, compared with pure argon, as manifested in the significant hypsochromic shifts of the CTML absorptions of both complex **2** (from ca. 552 nm in argon to ca. 536 nm in Ar/CO 3:1) and fragment **5** (from ca. 673 nm in argon to ca. 658 nm in 3:1 Ar/CO). Recall that in fluid solutions the CTML absorption bands of **1** and **2** experience a similar hypsochromic shift in going from cyclohexane to more polar solvents such as chloroform or acetonitrile.[11,13]

In a dinitrogen matrix, **2** undergoes photosubstitution of CO by the N_2 ligand, and this with a wavelength-dependent efficiency which parallels that of the CO photodissociation in the other matrices described above. In detail, long-wavelength irradiation through a 400 nm cutoff filter does not cause any reaction, even after 45 min, while increasingly efficient conversion of **2** occurs upon photolysis at 365, 313, and 289 nm. However, absorptions attributable to the fragment **5**, expected as the primary photoproduct, were not detectable, neither in the IR nor in the UV−vis spectrum. The latter shows a new CTML absorption emerging at 590 nm, while in the IR spectrum a three-band ν(CO) pattern (Figure 10, top) grows, along with weak absorptions (not shown in Figure 10) at 2140 cm^{-1} (free CO) and 2208 cm^{-1}. The latter feature is indicative of an end-on coordinated N_2 ligand, while the three-band ν(CO) pattern characterizes a *fac*-M(CO)$_3$ skeleton. Obviously, photolytic CO dissociation from **2** is immediately followed by taking up an N_2 molecule from the matrix environment into the vacant axial coordination site yielding *fac*-Mo(CO)$_3$(N_2)(iprop-dab) (**6**) (Scheme 11).

The analogous reaction of Mo(CO)$_3$(^{13}CO)(iprop-dab) (**2-*1a*/2-*1e***) with N_2 involves photodissociation of ^{13}CO or CO, yielding the unlabeled N_2 complex **6** along with its ^{13}CO-substituted derivatives **6-*1a*** and **6-*1e*** (Scheme 12). These two stereoisotopomers, unlike their precur-

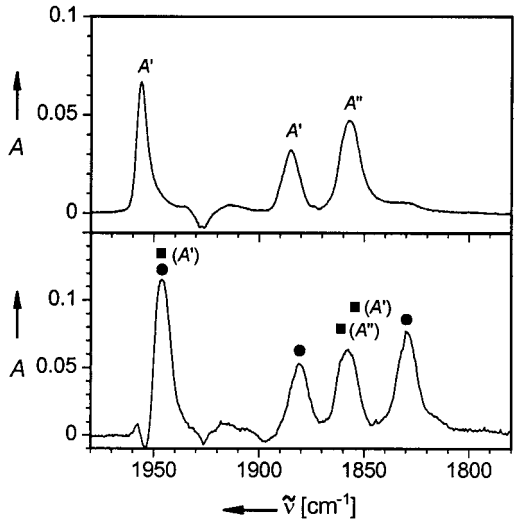

Figure 10. (top) CO stretching vibrational bands of *fac*-Mo(CO)$_3$(N$_2$)(iprop-dab) (**6**) generated from Mo(CO)$_4$(iprop-dab) (**2**) in a dinitrogen matrix by continued photolysis at 365 nm (25 min), 313 nm (10 min), and 289 nm (3 min; ca. 50% total conversion; note that the remaining absorptions of unreacted **2** have been removed by computer-assisted subtraction). (bottom) superimposed ν(CO) patterns of *fac*-Mo(CO)$_2$(ax-^{13}CO)(N$_2$)(iprop-dab) (**6-*1a***, ■) and *fac*-Mo(CO)$_2$-(eq-^{13}CO)(N$_2$)(iprop-dab) (**6-*1e***, ●) generated from Mo(CO)$_3$-(ax/eq-^{13}CO)(iprop-dab) (**2-*1a*/2-*1e***) in a dinitrogen matrix by continued photolysis at 365 nm (20 min), 313 nm (20 min), and 289 nm (5 min; ca. 60% total conversion; note that the remaining absorptions of unreacted **2-*1a*/2-*1e*** and those of concomitantly generated **6** have been removed by computer-assisted subtraction).

Scheme 11

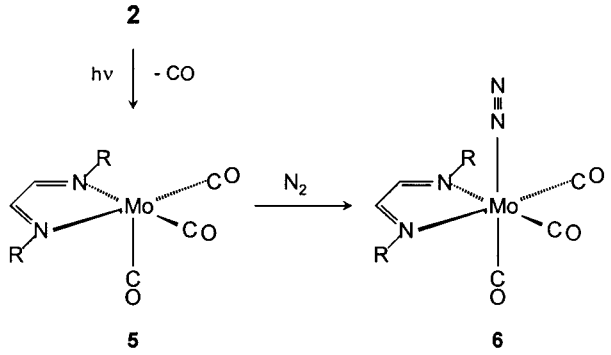

Scheme 12

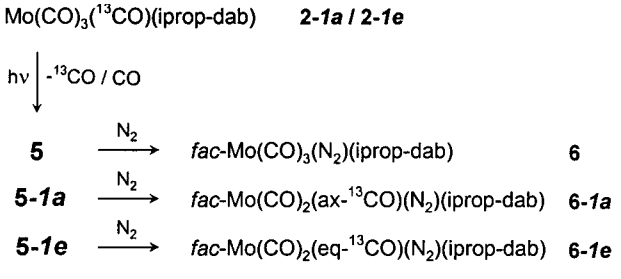

sors **5-*1a*** and **5-*1e*** (Figure 7, bottom), are clearly distinguishable on the basis of their ν(CO) patterns. The superimposed spectra of these two species are displayed in Figure 10 (bottom), which has been obtained from the actual reaction spectrum by means of computer-assisted subtraction of the absorptions associated with both the unreacted starting material and the unlabeled N$_2$ complex **6**. The individual assignments of bands to **6-*1a*** (marked ■) and **6-*1e*** (marked ●) are made on the basis of symmetry considerations (coincidence of the A″ ν(CO) modes of **6** and **6-*1a***) and with the help of the Teller−Redlich product rule.[55] The CO force field parameters, calculated[60] from the combined frequency data of **6** and its ^{13}CO-substituted derivatives (Table 5), show a considerable decrease of both k(ax) and k(eq) upon replacement of an axial CO group in **2** by the N$_2$ ligand, but again with a much more pronounced effect on the former (Table 5). This can largely be ascribed to the lower π acceptor capacity of N$_2$, which shares two metal d(π) orbitals with the remaining axial CO group but only one with each of the equatorial ones. Worth emphasizing in this context is the significant bathochromic shift of the CTML absorption band in going from **2** (540 nm in the N$_2$ matrix) to **6** (590 nm), which clearly reflects the substantial destabilization of the metal d(π) levels involved.

Flash Photolysis of Mo(CO)$_4$(iprop-dab) (2) in Solution at Ambient Temperature. In an exploratory study, both time-resolved IR and UV−vis spectroscopy have been employed to detect the *fac*-Mo(CO)$_3$(iprop-dab) fragment (**5**) as a transient species, generated from Mo(CO)$_4$(iprop-dab) (**2**) by laser flash photolysis (λ_{exc} = 308 or 248 nm) in cyclohexane solution at ambient temperature (Scheme 13).

Scheme 13

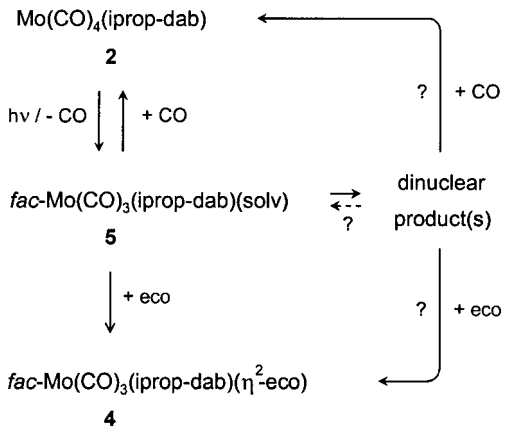

The CO stretching vibrational difference spectrum displayed in Figure 11 illustrates the situation 1.5 μs after 248 nm flash excitation of **2** (0.2 mM) in a rigorously deoxygenated cyclohexane solution under an argon atmosphere. It shows the depleted absorptions of the starting material at 2018, 1922, and 1874 cm^{-1} (see Table 1 for comparison with the data from a static spectrum of **2**) along with product bands emerging at 1944 and 1848 cm^{-1}. This pattern closely resembles the difference spectrum observed upon continuous photolysis of **2** in solid argon at 10 K (Figure 6, Table 5) and, hence, identifies the photogenerated species in solution as the CO loss product **5**, presumably present in solvated form, *fac*-Mo(CO)$_3$(iprop-dab)(solv) (solv = C$_6$H$_{12}$). Complementary UV−vis measurements (with 0.08 mM **2** in cyclohexane under an argon atmosphere; λ_{exc} 248 nm) expectedly show the instantaneous (submicrosecond time domain) depletion of the strong CTML absorption of **2**, centered at 562 nm in the static spectrum (see Table 3), while a new band appears in

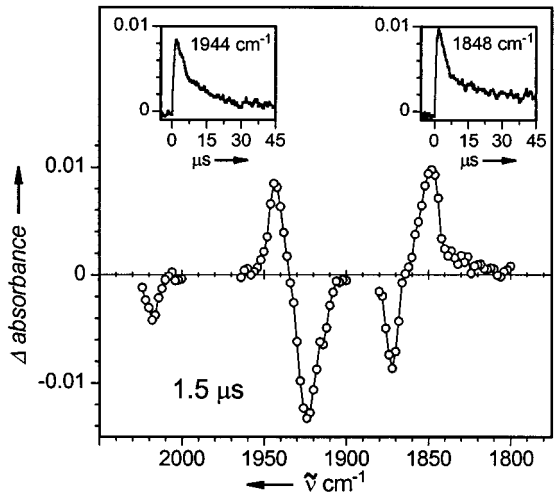

Figure 11. Transient ν(CO) IR difference spectrum recorded 1.5 μs after flash photolysis of $Mo(CO)_4$(iprop-dab) (**2**; 0.2 mM, λ_{exc} = 248 nm) in argon-saturated cyclohexane solution, showing the depleted bands of **2** (2018, 1922, and 1874 cm^{-1}) together with the absorptions of the photogenerated (solvated) $Mo(CO)_3$(iprop-dab) fragment **5** (1944 and 1848 cm^{-1}) and the subsequent decay of these bands (see insets).

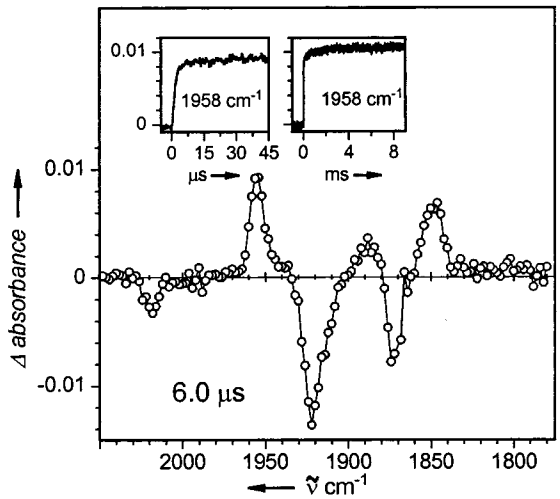

Figure 12. Transient ν(CO) IR difference spectrum recorded 6 μs after flash photolysis of $Mo(CO)_4$(iprop-dab) (**2**; 0.5 mM, λ_{exc} = 308 nm) in the presence of (*E*)-cyclooctene (20 mM) in argon-saturated cyclohexane solution, showing the depleted bands of **2** (2018, 1922, and 1874 cm^{-1}) together with the absorptions of photogenerated $Mo(CO)_3$(iprop-dab)(η^2-eco) (**4**) at 1956, 1888, and 1852 cm^{-1}, the emergence of which extends from microseconds (left inset) to milliseconds (right inset).

the 620−720 nm region. The latter compares well with the long-wavelength absorption of **5** in the argon matrix (Figure 8) and thus confirms the IR spectroscopic detection of this species in solution.

The fate of fragment **5** in the absence of potential ligands has not yet been clarified in detail. The two ν(CO) bands decay largely within 20−30 μs, with albeit ill-defined kinetics, as illustrated by the insets in Figure 11. However, inspection of the depletion bands reveals that recapturing of **5** by the photodissociated CO, with re-formation of **2**, plays only a minor role (<20%). Rather, the overall spectral changes lead to broad and unstructured absorptions at frequencies ranging from 1960 to 1935 cm^{-1} and from 1860 to 1800 cm^{-1} which do not yet allow a definite assignment but may tentatively be attributed to dinuclear product(s) (Scheme 13) such as $Mo_2(CO)_7$(iprop-dab)$_2$ and/or $Mo_2(CO)_6$(iprop-dab)$_2$. It should be mentioned as a useful hint in this context that continued photolysis of the homologous tungsten complex **1** in the absence of any potential ligand yields, among other decomposition products, a stable dinuclear compound of composition $W_2(CO)_6$(iprop-dab)$_2$ (by MS), which is currently under further investigation.

Time-resolved UV−vis spectroscopy reveals much less pronounced changes which, depending on the wavelength of observation in the visible region, extend from ca. 25 μs to ca. 1 ms. Consistent with the meager reformation of **2**, the depletion around 560 nm diminishes slightly by no more than 15−20%. Concomitant loss of intensity in the long-wavelength region around 620 nm amounts to 25−35%, thus indicating that **5** and its dinuclear decay product(s) exhibit closely overlapping CTML transitions, but with somewhat lower intensity of the latter species.

Trapping of photogenerated **5** (λ_{exc} = 308 nm) by added (*E*)-cyclooctene (with concentrations varied from 3 mM to 0.4 M) expectedly yields *fac*-$Mo(CO)_3$(iprop-dab)(η^2-eco) (**4**) as the sole final product, as monitored by IR spectroscopy in the ν(CO) region. However, this conversion proceeds in two batches involving different pathways (Scheme 13), with a branching ratio and with velocities depending on the concentration of (*E*)-cyclooctene. In experiments using low to medium (*E*)-cyclooctene concentrations (<10 mM), the decay of **5** is terminated within 15−20 μs and occurs with concomitant appearance of the major portion of **4** along with less intense ν(CO) absorptions associated with the aforementioned dinuclear decay product(s) of **5**. Further emergence of **4**, with concurrent decrease of the latter features, extends for milliseconds and thus indicates the partial involvement of the dinuclear species on the way from **5** to **4**. This second pathway is increasingly outmatched by the fast direct trapping of **5** at increasing concentrations of the olefin but is still recognizable even in the presence of 20 mM (*E*)-cyclooctene. This is illustrated in Figure 12, which shows, 6 μs after 308 nm flash excitation of **2** (0.5 mM) in cyclohexane solution containing 20 mM (*E*)-cyclooctene, the strong ν(CO) bands of **4** at 1956, 1888, and 1852 cm^{-1} (see Figure 1 for the static spectrum of **4**), while those of **5** have completely vanished. The two insets demonstrate that most of product **4** appears very rapidly, while an additional, albeit minor, portion is delivered subsequently within several milliseconds at the expense of the barely detectable transient absorptions in the 1840−1800 cm^{-1} region. Unfortunately, reliable disentangling of the kinetics of these processes is severely hindered by the spectral overlap of the involved species. Moreover, at medium to high concentrations of (*E*)-cyclooctene the decay of **5** becomes too rapid for the response time of our time-resolved IR instrumentation (~1 μs). Thus, in the above experiment with 20 mM (*E*)-cyclooctene the transient ν(CO) spectrum at 1 μs shows already the presence of both the fragment **5** and the ultimate product **4** in comparable concentrations.

Multicomponent kinetics, similarly unfavorable for disentangling, are also observed by means of time-resolved UV−vis spectroscopy, unless (*E*)-cyclooctene is present in such a high concentration that the side reaction(s) via the dinuclear transient species becomes negligible. In any case, the conversion of **5** into **4** ultimately leaves behind the broad band of **4** in the 600−740 nm region (Table 3; see Figure 4 for the closely related spectrum of the tungsten compound **3**) as a residual absorption, while the depletion in the 500−600 nm region experiences a substantial recovery due to the lower intensity of the CTML band of **4** compared with that of depleted **2** in this part of the spectrum (see Table 3). In an experiment with 0.4 M (*E*)-cyclooctene, all spectral changes are terminated within ca. 1.5 μs and the kinetic traces in either spectral region follow approximate first-order kinetics with $k_{obs} \approx 2.3 \times 10^6$ s^{-1} ($\tau_{1/2} \approx 0.3$ μs), yielding $k_{eco} = k_{obs}/c_{eco} \approx 5.8 \times 10^6$ L mol^{-1} s^{-1} as a reasonable estimate.

Carbon monoxide proved less efficient than (*E*)-cyclooctene for trapping photogenerated **5**. Even in CO-saturated solution, no more than ca. 60% recovery of **2** is observed by IR spectroscopy. Unfortunately, the decay of the ν(CO) absorptions of **5** does not provide clear-cut kinetic information (e.g., $\tau_{1/2} \approx 6$ μs measured at 1944 cm^{-1}, $\tau_{1/2} \approx 2$ μs measured at 1848 cm^{-1}) due to the spectral overlap with the concomitantly formed dinuclear side product(s). However, there is no doubt that, as discussed in the context of Scheme 6, recapturing of **5** solely by photodissociated CO, i.e., in the absence of added CO, is far too inefficient to compete noticeably with (*E*)-cyclooctene as the incoming ligand and, thus, to reduce the quantum yield for the photosubstitution of CO by the olefin under the actual conditions of the quantum yield determinations (15 mM concentration of (*E*)-cyclooctene).

Discussion

The photolytic loss of CO from **2** with formation of the *fac*-Mo(CO)$_3$(iprop-dab) fragment **5**, thought to exist in solvated form in hydrocarbon solution, parallels previous observations made with the related chromium complex Cr(CO)$_4$(bpy) in dichloromethane solution, where *fac*-Cr(CO)$_3$(bpy)(solv) was the only photoproduct detected by time-resolved IR spectroscopy.[85] However, in the latter case both LF and MLCT excitation proved effective, although not to the same extent.

It is appealing to correlate the selective loss of CO from an axial position of the M(CO)$_4$(α-diimine) complexes with the large difference between the axial and equatorial CO force constants in this type of compound (k(ax) − k(eq) amounts to 93.8 N m^{-1} in the case of Cr(CO)$_4$(bpy)[86] and 72.9 N m^{-1} in the case of **1** (Table 1) and varies from 84 to 93.9 N m^{-1} in the case of **2** (depending on the solvent or matrix material, Tables 1 and 5)). Despite some uncertainties arising from the counteractive effects of M←CO(σ) donation and M→CO(π*) back-donation on the C−O bond order,[87,88] it seems justified to assume that in the above cases the axial CO groups are less strongly bound to the metal than the equatorial ones (recall that the X-ray structure analysis of **2** shows indeed significantly longer axial Mo−CO distances).[61] Although this is a ground-state rather than an excited-state property, the same qualitative ordering of metal−CO bond strength may nevertheless be expected,[89] which should favor axial over equatorial CO photodissociation. Certainly, a *mer*-M(CO)$_3$(α-diimine) fragment in its ground state should be less stable and, hence, be disfavored compared with the corresponding *fac* isomer.[90]

Olefin ligands in group 6 carbonylmetal complexes commonly prefer an orientation that minimizes competition with other ligands for π back-donation from the metal and, thus, favors the metal d(π)→olefin (π*) component of the metal−olefin bond in the best possible way. Illustrative examples are the trans-orthogonal arrangement of two η^2-C═C units in various *trans*-M(CO)$_4$(η^2-olefin)$_2$[40,77,78] and *mer*-M(CO)$_3$(η^2:η^2-diene)(η^2-olefin)[45,48] compounds, the coplanar arrangement of the η^2-C═C and carbene unit in a *trans*-M(CO)$_4$(carbene)(η^2-olefin) complex,[42] the eclipsed orientation of the η^2-C═C unit to the L−M−L axis in compounds of the type *mer*-M(CO)$_3$(L)$_2$(η^2-olefin),[79,91] and the eclipsed orientation of the η^2-C═C unit to a L−M−CO axis in *mer*-M(CO)$_3$(L−L)(η^2-olefin)[62,80,92] and *cis*-M(CO)$_4$(L)(η^2-olefin)[91,93] systems. With these precedents in mind, one might suspect that a *mer*-M(CO)$_3$(iprop-dab)(η^2-eco) geometry of **3** and **4** (where the η^2-C═C unit, if eclipsed to one of the N−M−CO axes, shares a metal d(π) orbital with only one carbonyl ligand) would be thermodynamically favored over the actually observed structure (Figure 3), where the olefin experiences competitive demand for π back-donation from the metal by two carbonyls and by the α-diimine ligand. If so,[90] a very high barrier should exist which prevents the *fac*-M(CO)$_3$(iprop-dab)(η^2-eco) complexes from skeletal rearrangement to the respective *mer* isomers. Worth mentioning in this context is the well-documented (vide supra) rigidity of the *fac*-W(CO)$_2$(eq′/eq″-^{13}CO)(iprop-dab)(η^2-eco) stereoisotopomers (**3-*1e*′**/**3-*1e*″**) which indicates that, despite the very rapid olefin rotation in the axial position, a skeletal rearrangement with axial−equatorial ligand exchange is indeed strongly hindered.

Somewhat puzzling, at first sight, is the fact that both **3** and **4** fail to undergo secondary CO photosubstitution in the presence of excess (*E*)-cyclooctene, although the existence of M(CO)$_2$(α-diimine)(η^2-olefin)$_2$ complexes[34−38] is well documented and, moreover, the occurrence of photolytic CO dissociation from **3** is obvious from the observation of the photoinitiated ^{13}CO enrichment. However, close examination of this latter process (Scheme 4) reveals that ^{13}CO from the bulk solution is selectively introduced into the equatorial positions. Should this also

(85) Virrels, I. G.; George, M. W.; Turner, J. J.; Peters, J.; Vlček, A., Jr. *Organometallics* **1996**, *15*, 4089−4092.
(86) Vlček, A., Jr.; Grevels, F.-W.; Snoeck, T. L.; Stufkens, D. J. *Inorg. Chim. Acta* **1998**, *287*, 83−90.
(87) Elschenbroich, C.; Salzer, A. *Organometallchemie*; Teubner: Stuttgart, Germany, 1990.
(88) Willner, H.; Aubke, F. *Angew. Chem.* **1997**, *109*, 2506−2530; *Angew. Chem., Int. Ed. Engl.* **1997**, *36*, 2402−2405.
(89) Dahlgren, R. M.; Zink, J. I. *Inorg. Chem.* **1977**, *16*, 3154−3161.
(90) A comparative DFT study of *fac*- and *mer*-Mo(CO)$_3$(iprop-dab) and related species is in progress (collaboration with G. Olbrich of the MPI für Strahlenchemie) and will be published in a forthcoming paper.
(91) Koemm, U.; Kreiter, C. G.; Strack, H. *J. Organomet. Chem.* **1978**, *148*, 179−200.
(92) Kreiter, C. G.; Koemm, U. *Z. Naturforsch., B* **1983**, *38*, 943−952.
(93) Kreiter, C. G.; Strack, H. *Z. Naturforsch., B* **1975**, *30*, 748−750.

be applicable to (*E*)-cyclooctene as the entering ligand, the resulting product would contain two η^2-coordinated olefins in positions cis to each other. This type of arrangement, although known from a variety of *cis*-$M(CO)_4(\eta^2\text{-olefin})_2$ and *fac*-$M(CO)_3(\eta^{2:2}\text{-dien})(\eta^2\text{-olefin})$ complexes,[44,48,94,95] is, however, noted for its low or, at best, moderate thermal stability. In other words, we cannot exclude that $W(CO)_2$(iprop-dab)-*cis*-$(\eta^2\text{-eco})_2$ is generated as an unstable product but then does not survive due to replacement of the second η^2-eco ligand by photodissociated CO with re-formation of **3**, so that no net conversion is detectable.

What deserves particular attention is the influence of the olefin ligand in **3** and **4** on the electronic transitions in the CTML region. As illustrated in Figure 4 and documented in Table 3, replacement of CO in **1** and **2** by (*E*)-cyclooctene leads to a small shift of the dominant CTML absorption band to shorter wavelength from 549 to 520 nm in the case of tungsten and from 562 to 558 nm in the case of molybdenum. However, in either case this transition experiences a substantial loss of intensity in favor of a new broad absorption band emerging at the lower energy side centered around 650 and 690 nm, respectively. We attribute this to the single-face π-acceptor character of the olefin ligand. Recall that two metal d(π) orbitals are available for π back-donation into the axial positions. The olefin, unlike CO, makes use of only one of them, thus leaving the other one unused and, hence, destabilized. As a consequence of this, one transition of the CTML manifold is shifted to lower energy, thus giving rise to a broad band around 650 nm (**3**) or 690 nm (**4**) and, moreover, to the reduced intensity of the remaining absorption at 520 nm (**3**) or 558 nm (**4**).

Experimental Section

General Considerations. All reactions and manipulations were carried out under argon and in argon-saturated solvents, unless otherwise noted. Photochemical reactions on a preparative scale were carried out in a water-cooled immersion-well apparatus[96] (Solidex glass, $\lambda > 280$ nm) equipped with a Philips HPK 125-W high-pressure mercury lamp.

Solution spectra were recorded on the following instruments: IR, Perkin-Elmer 1600 (operating with 2 cm^{-1} resolution) or Bruker IFS 66 (operating with 0.5 cm^{-1} resolution); UV−vis, Bruins Instruments Omega 10 or Shimadzu UV-2102PC; NMR, Bruker ARX 250, DRX 400, or DRX 500; MS, Finnigan MAT 8200.

Reagents. Analytical grade and deuterated solvents (Merck, Darmstadt, Germany) were used as received. ^{13}CO was purchased from Cambridge Isotope Laboratories (CLM-1845: 99% ^{13}C, <1% ^{18}O) via Promochem (Wesel). High-purity gases for low-temperature matrix experiments (Ar, ≥99.9999%; CO, ≥99.997%, N_2, ≥99.9995%) were purchased from Messer-Griesheim. (*E*)-Cyclooctene[97,98] (eco) and 1,4-diisopropyl-1,4-diazabuta-1,3-diene[81,99,100] (iprop-dab; mp 58−59 °C, sealed capillary) were prepared by adapting the published procedures. $Mo(CO)_4$(iprop-dab) (**2**; mp 154−155 °C, sealed capillary; for ν(CO) IR and ^{13}C NMR data, see Tables 1 and 2) was generated from $Mo(CO)_6$ and iprop-dab by irradiation in toluene solution at ambient temperature, followed by recrystallization from toluene/hexane (ca. 90% yield). The analogous preparation of $W(CO)_4$(iprop-DAB) (**1**; mp 161−162 °C, sealed capillary; for ν(CO) IR and ^{13}C NMR data, see Tables 1 and 2) required heating to 60 °C, after the irradiation, to convert the photochemically generated monodentate complex $M(CO)_5$(iprop-dab)[81] into the desired chelate tetracarbonyl product (ca. 80% yield).

***fac*-W(CO)$_3$(iprop-dab)(η^2-eco) (3).** A solution of $W(CO)_4$-(iprop-dab) (**1**; 0.44 g, 1.0 mmol) and (*E*)-cyclooctene (0.78 mL, 0.66 g, 6.0 mmol) in cyclohexane (400 mL) was irradiated until the ν(CO) IR bands of **1** disappeared completely (90 min). Vacuum evaporation of the solvent yielded spectroscopically pure **3** as a dark purple solid (0.48 g, 93%). For complete characterization this material was recrystallized by dissolving it in 20 mL of toluene containing 0.5% (*E*)-cyclooctene, to which 20 mL *n*-hexane was added before cooling to dry ice temperature to precipitate dark purple crystals: mp 143−145 °C (sealed capillary). IR ν(CO) data (*n*-hexane): 1964.9 (vst), 1901.3 (m), ∼1893 (sh), 1860.8 (st), ∼1855 (wsh) cm^{-1}; for the data in cyclohexane see Table 1. UV−vis: see Table 3. ^1H NMR (toluene-d_8, 300 K): δ 7.697 (=CH−, s), 7.472 (=CH−, s), 4.045 (−CH<, sept, 6.6 Hz), 3.895 (−CH<, sept, 6.5 Hz), 1.214 ($-CH_3$, d, 6.2 Hz), 1.199 ($-CH_3$, d, 6.2 Hz), 1.158 ($-CH_3$, d, 6.5 Hz), and 0.862 ($-CH_3$, d, 6.6 Hz) for the iprop-dab ligand; δ 3.046 (2 =CH−, m), ∼2.06 (2 H, m), ∼1.82 (2 H, m), ∼1.74 (2 H, m), ∼1.33 (2 H, m), ∼0.78 (2 H, m), and ∼0.61 (2 H, m) for the η^2-eco ligand. ^{13}C NMR (dichloromethane-d_2, 300 K): δ 224.58 and 223.77 (CO-eq), 213.14 (CO-ax), 153.35 and 152.75 (−CH=N−), 84.43 ($-CH_2CH$=), 66.65 and 63.82 (=NCH<), 37.44, 37.26, and 29.42 ($-(CH_2)_3CH$=), 26.84, 25.24, 24.47, and 22.91 ($-CH_3$); for the data in toluene-d_8 see Table 2. Anal. Calcd for $C_{19}H_{30}N_2O_3W$ (M_r = 518.4): C, 44.03; H, 5.83; N, 5.40; W, 35.47. Found: C, 43.88; H, 5.81; N, 5.26; W, 34.99.

W(CO)$_3$(^{13}CO)(iprop-dab) (1-*1*). A solution of *fac*-$W(CO)_3$-(iprop-dab)(η^2-eco) (**3**; 0.08 g, 0.15 mmol) in cyclohexane (100 mL) under a ^{13}CO atmosphere (100 mL, 1 bar) was stirred at 40 °C until the ν(CO) pattern of **3** disappeared completely (30 h). Vacuum evaporation of the solvent yielded **1-*1*** as a solid material, identified on the basis of the ^{13}C NMR spectrum (chemical shifts identical with those of **1** (cf. Table 2), but with much higher intensity of the carbonyl signal, which also showed the satellite lines arising from coupling with ^{183}W), the MS data (90% mono-^{13}CO), and the IR ν(CO) pattern (total number of eight bands (see Table 1), as expected for the two positional isotopomers of **1-*1*** (**1-*1a*** and **1-*1e***)).

^{13}CO-Enriched Samples of W(CO)$_3$(iprop-dab)(η^2-eco) (3-#).[53] (a) Photolysis of 3 under a ^{13}CO Atmosphere. A solution of $W(CO)_3$(iprop-dab)(η^2-eco) (**3**; 0.08 g, 0.15 mmol) in cyclohexane (100 mL) was stirred under a ^{13}CO atmosphere (100 mL, 1 bar) and irradiated until the desired conversion of the starting material was achieved (e.g., 23% after 5 min, yielding the sample described below), as monitored by IR spectroscopy. After vacuum evaporation of the solvent, chromatography on silica (Merck, 0.2−0.063 mm; column with d = 2.5 cm and l = 30 cm) with toluene as the eluent was employed to remove traces of byproducts (second fraction, discarded) from **3-#** (first fraction), which was identified on the basis of its ^{13}C NMR spectrum (chemical shifts identical with those of **3** (see Table 2), but with varying intensities of

(94) Gregory, M. F.; Jackson, S. A.; Poliakoff, M.; Turner, J. J. *J. Chem. Soc., Chem. Commun.* **1986**, 1175−1177.
(95) Weiller, B. H.; Grant, G. R. *J. Am. Chem. Soc.* **1987**, *109*, 1252−1253.
(96) Grevels, F.-W.; Reuvers, J. G. A.; Takats, J. *Inorg. Synth.* **1986**, *24*, 176−180.
(97) Vedejs, E.; Snoble, K. A. J.; Fuchs, P. L. *J. Org. Chem.* **1973**, *38*, 1178−1183.
(98) Inoue, Y.; Tsuneishi, H.; Hakushi, T.; Tai, A. In *Photochemical Key Steps in Organic Synthesis: An Experimental Course Book*; Mattay, J., Griesbeck, A., Eds.; VCH: Weinheim, Germany, 1994; p 207.
(99) Kliegman, J. M.; Barnes, R. K. *Tetrahedron* **1970**, *26*, 2555−2560.
(100) Svoboda, M.; tom Dieck, H.; Krüger, C.; Tsay, Y.-H. *Z. Naturforsch., B* **1981**, *36*, 814−822.

the carbonyl resonances at δ 224.10 (singlet, 58.5% relative intensity (rel int); with satellites from coupling to ^{183}W, J = 147 Hz), 223.86 (singlet, 28% rel int), 213.15 (singlet with 4.5% rel int and superimposed doublet, J = 4.5 Hz, with 9% rel int)) and further characterized by IR spectroscopy (see Figure 2, top).

(b) Photoreaction of 1-*1* with (*E*)-Cyclooctene. A solution of W(CO)$_3$(^{13}CO)(iprop-dab) (**1-*1***; 0.04 g, 0.09 mmol) and (*E*)-cyclooctene (0.3 mL, 0.26 g, 2.3 mmol) in cyclohexane (95 mL) was irradiated (3.5 min) until 85% conversion of the starting material was observed by IR spectroscopy. After vacuum evaporation of the solvent, column chromatography on silica (Merck, 0.2−0.063 mm; cooled column, −30 °C, d = 2.5 cm, l = 30 cm) with toluene as the eluent was employed to separate residual **1-*1*** (second fraction) from **3-#** (first fraction), which was identified on the basis of its ^{13}C NMR spectrum (chemical shifts identical with those of **3** (see Table 2), but with strongly enhanced carbonyl resonances at δ 224.10 (s), 223.86 (s), and 213.15 (singlet with superimposed weak doublet, $J \approx$ 5 Hz) which exhibit 35:33:32 relative intensities and show satellite lines arising from coupling with ^{183}W) and further characterized by IR spectroscopy (ν(CO) absorptions attributed to **3**, **3-*1a***, and **3-*1e′*/3-*1e″***, as listed in Table 1).

***fac*-Mo(CO)$_3$(iprop-dab)(η^2-eco) (4).** A solution of Mo(CO)$_4$(iprop-dab) (**2**; 0.35 g, 1.0 mmol) and (*E*)-cyclooctene (0.78 mL, 0.66 g, 6.0 mmol) in cyclohexane (430 mL) was irradiated until the ν(CO) IR bands of **2** disappeared completely (2.5 h). Vacuum evaporation of the solvent from the filtered solution yielded spectroscopically pure **4** as a violet solid material (0.36 g, 84%). For complete characterization this material was recrystallized by dissolving it in 40 mL of toluene containing 3% (*E*)-cyclooctene, to which 40 mL of *n*-hexane was added before cooling to dry ice temperature to precipitate violet crystals, mp 150−151 °C (sealed capillary). IR ν(CO) data (in *n*-hexane containing 5% (*E*)-cyclooctene): 1958.0 (vst, with sh at ∼1956), 1893.4 (m), 1886.4 (m), 1854.7, and ∼1850 (sh) cm^{-1}; see Figure 1. UV−vis: see Table 3. ^{13}C NMR: see Table 2. Anal. Calcd for $C_{19}H_{30}MoN_2O_3$ (M_r = 430.4): C, 53.02; H, 7.03; N, 6.51; Mo, 22.29. Found: C, 53.15; H, 7.08; N, 6.60; Mo, 22.41.

Mo(CO)$_3$(^{13}CO)(iprop-dab) (2-*1*). A solution of *fac*-Mo(CO)$_3$(iprop-dab)(η^2-eco) (**4**; 50 mg) in cyclohexane (100 mL) was stirred under a ^{13}CO atmosphere (100 mL, 1 bar) at ambient temperature until the ν(CO) pattern of **4** disappeared completely (4.8 h). Vacuum evaporation of the solvent yielded **2-*1*** as a solid material (40 mg), identified on the basis of the ^{13}C NMR spectrum (chemical shifts identical with those of **2** (see Table 2), but with much higher intensities of the two carbonyl signals), the MS data (92% mono-^{13}CO), and the IR ν(CO) pattern (total number of eight bands (Table 1), as expected for the two positional isotopomers of **2-*1*** (**2-*1a*** and **2-*1e***)).

X-ray Diffraction and Crystal Data of *fac*-W(CO)$_3$(iprop-dab)(η^2-eco) (3). Crystals of **3** were grown from *n*-hexane. Crystal data and data collection and refinement details: $C_{19}H_{30}N_2O_3W$, M_r = 518.30, violet-black needles, crystal size 0.33 × 0.04 × 0.03 mm, orthorhombic, a = 19.458(1) Å, b = 7.6604(5) Å, c = 13.446(1) Å, U = 2004.1(4) Å^3, T = 100 K, $Pna2_1$ (No. 33), Z = 4, d_{calcd} = 1.72 Mg·m^{-3}, μ = 5.783 mm^{-1}, Siemens SMART-CCD diffractometer, λ = 0.710 73 Å, CCD-ω scan, 21 238 measured reflections, 7099 independent, 3949 observed ($I > 2\sigma(I)$), F(000) = 1024 e, [(sin θ)/λ]$_{max}$ = 0.97, Gaussian absorption correction (T_{min} = 0.69877; T_{max} = 0.84093), direct methods (SHELXS-97),[101] least-squares refinement on F_o^2 using Chebyshev weights (SHELXL-97),[101] W and O anisotropic, a methyl group of one of the isopropyl groups is disordered over two positions (50:50) and was modeled by two isotropic C atoms, each with half-occupancy (C15A, C15B), nondisordered H atoms riding, otherwise omitted, 125 refined parameters, R1 = 0.057 (observed data), wR2 = 0.114 (all data), final shift/error 0.001, residual electron density 2.246 e Å^{-3} (0.847 Å from W).

Quantum Yields. Light absorption was measured by means of a modified version of an electronically integrating actinometry device,[102] which provides a numerical value for the total amount of light absorbed by the system, $\int_0^t Q_{abs}\,dt$ (einstein L^{-1}), and thus eliminates any problems arising from nonconstant incident photon fluxes and/or incomplete absorption of light in the sample cell. The instrument was calibrated using Actinochrome N (*meso*-diphenylhelianthrene)[103] at 548 nm and ferrioxalate actinometry[104] at the other wavelengths of excitation. Irradiation of 3.0 mL aliquots of carefully deaerated stock solutions of complexes **1** and **2** (ca. 1 mM) in cyclohexane containing (*E*)-cyclooctene (ca. 15 mM) was carried out at 23 ± 1 °C in quartz cuvettes (d = 1 cm) by using a Hanovia 1000 W Hg−Xe lamp connected to a Schoeffel Instruments GM 252 grating monochromator. Light intensities were of the order of (0.6−1.8) × 10^{-6} einstein min^{-1} absorbed by the 3.0 mL samples. Quantitative IR spectroscopy (PE 1600 instrument; IR cell with CaF_2 windows, d = 508 μm) was employed to determine the concentrations of the involved complexes on the basis of the following molar absorbance data: **1**, ϵ = 6378 L mol^{-1} cm^{-1} at 2016.7 cm^{-1}; **2**, ϵ = 5381 L mol^{-1} cm^{-1} at 2019.3 cm^{-1}; **3**, ϵ = 8722 L mol^{-1} cm^{-1} at 1963.0 cm^{-1}; **4**, ϵ = 8567 L mol^{-1} cm^{-1} at 1956.9 cm^{-1}. The UV−vis molar absorbance data used to account for mutual internal filtering in the evaluation of the quantum yields[82,83] at 254, 302, 365, and 405 nm are listed in Table 4.

Low-Temperature Matrix Photochemistry. The basic setup consists of a CaF_2 window mounted with indium gaskets in a copper holder attached to the end stage of an Air Products CS202 Displex refrigerator. Details of the equipment used for controlling the temperature (10 K), flow of matrix gas (usually 1.5−2 mmol h^{-1}), and metal complex deposition rate by incorporated microcrystal balance have been reported previously.[105,106] Narrow- and broad-band irradiation light is selected from the output of a 1000 W Hg/Xe lamp by means of a Schoeffel GM 252 monochromator, with selected cutoff filters as an added precaution. For some experiments a Perkin-Elmer 580 IR grating spectrometer was used, but in most experiments the Perkin-Elmer 1760 FTIR and PE330 spectrometers were employed for IR and UV−vis spectroscopy, respectively. Complex **2** was evaporated from a heatable glass inlet source separately outgassed at 200 °C. The evaporation temperature (75 °C) was selected to achieve a guest:host ratio of <1:1000.

Laser Flash Photolysis. The basic design of the instrumentation for flash photolysis in combination with time-resolved IR spectroscopy has been described elsewhere.[107] The actual configuration used in the present study involves a Lambda Physik EMG 200 excimer laser (with XeCl for λ = 308 nm; pulse duration 20 ns, energy attenuated to 50 mJ/pulse) and a Lambda Physik EMG 201 MSC excimer laser (with KrF for λ = 248 nm; 15 ns pulse duration, energy attenuated to 7 mJ/pulse) as the excitation light sources, focused by means of a cylindrical quartz lens in order to illuminate a 1−2 mm wide area of the sample cell. A globar in combination with a Spex double monochromator, arranged as described previously,[107] serves as the IR monitoring light source. For time-resolved signal detection, amplifying, and

(101) Sheldrick, G. M. SHELXL-97; University of Göttingen, Göttingen, Germany, 1997.

(102) Amrein, W.; Gloor, J.; Schaffner, K. *Chimia* **1974**, *28*, 185−188.

(103) Brauer, H. D.; Schmidt, R.; Gauglitz, G.; Hubig, S. *Photochem. Photobiol.* **1983**, *37*, 595−598.

(104) (a) Hatchard, C. G.; Parker, C. A. *Proc. R. Soc. London, Ser. A* **1956**, *235*, 518−536. (b) Murov, S. L. *Handbook of Photochemistry*; Dekker: New York, 1973; p 119.

(105) Gerhartz, W.; Grevels, F.-W.; Klotzbücher, W. E. *Organometallics* **1987**, *6*, 1850−1856.

(106) Klotzbücher, W. E. *Cryogenics* **1983**, *23*, 554−556.

(107) Schaffner, K.; Grevels, F.-W. *J. Mol. Struct.* **1988**, *173*, 51−65.

storage, a HgCdTe photodiode (HCT-6-7, Infrared Associates Inc.; $D^*_{max} = 6 \times 10^{10}$ cm $Hz^{1/2}$ W^{-1}) was used in combination with a Polytec PPA-15-DC preamplifier and a Tektronix AM 502 main amplifier (providing for an overall amplification by a factor of 14 000 with a system response time on the order of 1 μs) and a digital storage oscilloscope (Gould 4072, 100 MHz, 400 Ms s^{-1}). An Atari 1040 ST computer, operating with homemade software written in Ansi-C, was employed for data averaging and storage prior to kinetic analysis and point-by-point construction of spectra on a VAX/VMS computer (Digital Inc.) by means of homemade software written in Fortran 77. The sample cell (CaF_2 windows, $d = 1$ mm), thermostated to 25 °C, was connected to a reservoir containing the stock solution. The routine procedure for preparing the sample solution involved ca. 10% liquid pumping, followed by saturation with the desired gas from an attached gas reservoir kept at ca. 1.06 bar constant pressure. After each laser shot, the sample cell was emptied, flushed with the respective gas, and refilled with fresh stock solution from the reservoir via a magnetic valve system.

Samples for the UV−vis monitored flash photolysis, with rectangular arrangement of excitation and monitoring beams, were analogously prepared and placed in a 1 × 1 cm quartz cuvette.

Acknowledgment. Thanks for skillful technical assistance are due to P. Bayer, L. J. Currell, C. Laurich, (Mrs.) D. Merkl, and the NMR spectroscopic staff of the MPI für Strahlenchemie. Financial support by the Alexander von Humboldt-Stiftung is gratefully acknowledged (S.Ö.). We thank Prof. R. Schmidt (Universität Frankfurt/Main) for a generous gift of Actinochrome N (*meso*-diphenylhelianthrene), Dr. W. Schrader and coworkers (MPI für Kohlenforschung) for carrying out the MS analyses, and Dr. H. Görner (MPI für Strahlenchemie) for support and advice concerning time-resolved IR and UV−vis spectroscopy.

Supporting Information Available: Tables of X-ray data collection information, atomic coordinates, thermal parameters, and bond lengths and angles, together with crystallographic data files in CIF format, for **3**. This material is available free of charge via the Internet at http://pubs.acs.org.

OM010410B